Chapter 9

The ocean and its circulation

We now begin our discussion of the circulation of the ocean. In this introductory chapter we describe the physical characteristics of the ocean, the properties of sea water, its global-scale temperature and salinity distributions and the geography of the basins in which it is contained. We go on to describe, and interpret in terms of the balanced — geostrophic and hydrostatic — dynamics of Chapter 7, the observed pattern of ocean currents. Those readers who have a primary interest in ocean circulation and have not read all the way through to here, will find essential dynamical background reviewed in Chapters 6 and 7, to which frequent reference is made.

The ocean, like the atmosphere, is a stratified fluid on the rotating Earth. The two fluids have many similarities in their behavior and, especially, in their fluid dynamics. However, there are some important differences:

- The fluids are physically different: water is (almost) incompressible and ocean thermodynamics has no counterpart of atmospheric moisture (as a source of latent heat).

- Unlike the atmosphere, all oceans are laterally bounded by continents — see Fig.9.1 — except in the Southern Ocean where the ocean extends all the way around the globe and fluid can pass through Drake Passage, the narrow (600 km) gap between the tip of South America and the Antarctic peninsula.

- The ocean circulation is forced in a different way from the atmosphere. We have seen that the atmosphere is largely transparent to solar radiation and is heated from below by convection. By contrast, the ocean

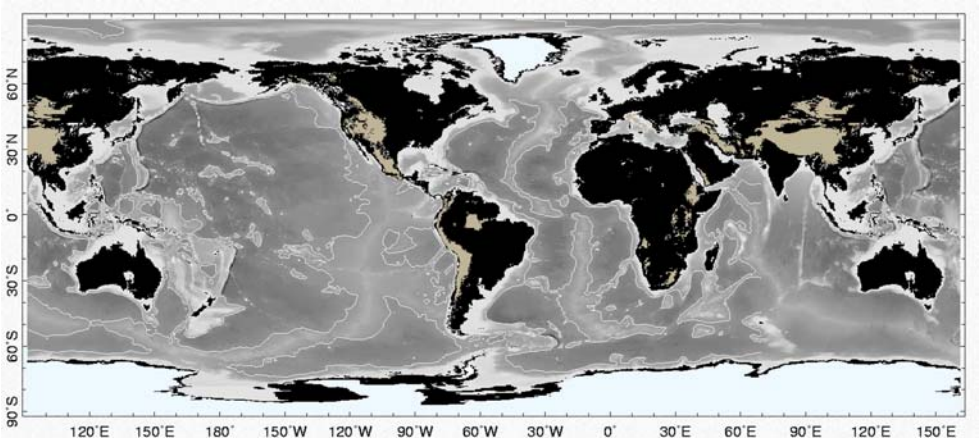

Figure 9.1: World relief showing elevations over land and ocean depth. White areas over the continents mark the presence of ice at altitudes that exceed 2 km. The mean depth of the ocean is 3.7 km, but depths sometimes exceed 6 km. The thin white line meandering around the ocean basins marks a depth of 4 km.

exchanges heat and moisture with the atmosphere at its upper surface; convection in the ocean is driven by buoyancy loss *from above*[1]. In addition, there is a very important process forcing the ocean circulation that has no counterpart in the atmosphere. Winds blowing over the ocean surface exert a *stress* on it. The wind is a major driver of ocean circulation, particularly in the upper kilometer or so.

The wind-driven and buoyancy-driven circulations are intimately intertwined. Nevertheless, for pedagogical reasons here we discuss them separately, devoting Chapter 10 to the former and Chapter 11 to the latter. Finally, in Chapter 12, we discuss the role of the ocean in climate and paleoclimate.

[1] There are sources of geothermal heating at the bottom of the ocean but, in an average sense, this accounts for only a few milliwatts/m^2 of heat input, compared to air-sea heat fluxes of ± 10 to 100W/m^2 — see Chapter 11.

surface area	$3.61 \times 10^{14}\,\mathrm{m}^2$
mean depth	$3.7\,\mathrm{km}$
volume	$3.\,2 \times 10^{17}\,\mathrm{m}^3$
mean density	1.035×10^3 kg m^{-3}
ocean mass	$1.3 \times 10^{21}\,\mathrm{kg}$

Table 9.1: Some key ocean numbers.

salt	$^o/_{oo}$ $\left(\mathrm{g\,kg^{-1}}\right)$
chloride	18.98
sodium	10.56
sulphate	2.65
magnesium	1.27
calcium	0.40
potassium	0.38
bicarbonate	0.14
others	0.11
overall salinity	34.48

Table 9.2: Major constituents of sea water. The *relative proportion* of the dissolved salts tabulated here does not vary much from place to place. This is because salts largely come from weathering of continents which is a very slow input compared to the mixing rate of the whole ocean (100,000 years compared to 1000 years).

9.1 Physical characteristics of the ocean

9.1.1 The ocean basins

The ocean covers about 71% of the Earth's surface and has an average total depth of 3.7 km; the distribution of land and sea and the bathymetry of the ocean basins is plotted in Fig.9.1. A north-south section along the Greenwich meridian through Fig.9.1 is shown in Fig.1.2. We see that the ocean basins are highly complex and the bottom topography much more jagged than that of the land surface — see also the bathymetry shown in the hydrographic section of Fig.9.9. This is because, as we shall see, abyssal ocean currents

specific heat	c_w	4.18×10^3	J kg^{-1} K^{-1}
latent heat of fusion	L_f	3.33×10^5	J kg^{-1}
latent heat of evaporation	L_e	2.25×10^6	J kg^{-1}
density of fresh water	ρ_{fresh}	0.999×10^3	kg m^{-3}
viscosity	μ_{water}	10^{-3}	kg m^{-1} s^{-1}
kinematic viscosity	$\nu = \frac{\mu_{water}}{\rho}$	10^{-6}	m^2 s^{-1}
thermal diffusivity	k	1.4×10^{-7}	m^2 s^{-1}

Table 9.3: Physical properties of liquid water.

are, in the mean, weak and temperature changes very slight, so the erosion of submarine relief by ocean currents occurs at a much slower rate than that of the mountains on land.

The volume of the oceans is 3.2×10^{17} m^3, a huge amount of water totalling roughly 1.3×10^{21} kg — see Table 9.1 — with a correspondingly enormous heat capacity, 1000 times that of the atmosphere. As discussed in Chapter 12.1, this is one of the reasons that the ocean plays such an important role in climate.

9.1.2 The cryosphere

About 2% of the water on the planet is frozen and is known as the "cryosphere" (from the Greek '*kryos*', meaning frost or cold). It includes ice sheets, sea ice, snow, glaciers and frozen ground (permafrost). Most of the ice is contained in the ice sheets over the landmasses of Antarctica (89%) and Greenland (8%). These sheets store about 80% of the freshwater on the planet. The Antarctic ice sheet has an average depth of about 2 km (Fig.1.2); the Greenland ice sheet is some 1.5 km thick. Of great importance for climate is not so much the mass of ice but rather the surface area covered by it. The albedo of ice can be very high, reaching 70% (see Table 2.2 and Fig.2.4), and so reflects much of the radiation incident on it. Perennial (year-round) ice covers 11% of the land area and 7% of the ocean. Moreover, sea ice is also important because it regulates exchange of heat, moisture and salinity in the polar oceans and insulates the relatively warm ocean water from the cold polar atmosphere.

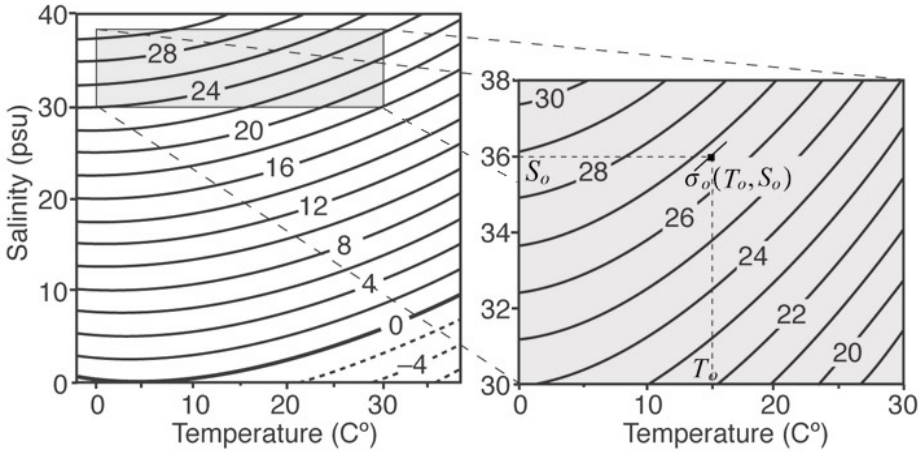

Figure 9.2: Contours of seawater density anomalies ($\sigma = \rho - \rho_{ref}$ in $\mathrm{kg\,m^{-3}}$) plotted against salinity (in psu = $\mathrm{g\,kg^{-1}}$) and temperature ($^\circ$C) at the sea surface. Note that sea water in the open ocean has σ in the range 20 to 29 $\mathrm{kg\,m^{-3}}$, T in the range $0 - 30\,^\circ$C and S in the range $33 - 36$ psu. The panel on the right zooms in on the region of oceanographic relevance. An approximation to the equation of state in the vicinity of the point $\sigma_o(T_o, S_o)$ is given by Eq.(9.5).

9.1.3 Properties of seawater; equation of state

Some key properties of water are set out in Table 9.3. The density of pure water at $4\,^\circ$C is 0.999×10^3 $\mathrm{kg\,m^{-3}}$. The mean density of sea water is only slightly larger, $1.035 \times 10^3\,\mathrm{kg\,m^{-3}}$. Unlike air, the density of sea water varies rather little — by only a few % — but, as we shall see, these variations turn out to be central to the dynamics. Cold water is denser than warm water; salty water is denser than fresh water; pressure increases the density of water. Density depends on temperature T, salinity S and pressure p in a rather complicated, non-linear way (deduced by very careful laboratory measurements) which we represent symbolically as:

$$\rho = \rho(T, S, p). \tag{9.1}$$

Salinity is a measure of the amount of salt dissolved in the water, about 85% of which is sodium and chloride — see Table 9.2. Modern salinity measurements are dimensionless: the 'Practical Salinity Scale' defines salinity in terms of a conductivity ratio very nearly equal to $\mathrm{g\,kg^{-1}}$ or, equivalently, $^o/_{oo}$

Surface			
T_o (°C)	-1.5	5	15
α_T $\left(\times 10^{-4}\,\mathrm{K}^{-1}\right)$	0.3	1	2
S_o (psu)	34	36	38
β_S $(\times 10^{-4}\mathrm{psu}^{-1})$	7.8	7.8	7.6
σ_o $(\mathrm{kg\,m}^{-3})$	28	29	28
Depth of 1 km			
T_o (°C)	-1.5	3	13
α_T $\left(\times 10^{-4}\,\mathrm{K}^{-1}\right)$	0.65	1.1	2.2
S_o (psu)	34	35	38
β_S $(\times 10^{-4}\mathrm{psu}^{-1})$	7.1	7.7	7.4
σ_o $(\mathrm{kg\,m}^{-3})$	-3	0.6	6.9

Table 9.4: The dependence of σ, α_T and β_S on T and S at two levels in the ocean, at the surface and a depth of 1km.

(parts per thousand). Typically, seawater has a salinity of 34.5psu ('practical salinity units' or 'psu' for short): thus one kg of seawater typically has 34.5 g of salt dissolved in it. Seawater is almost incompressible; not quite, since at enormous pressures in the interior ocean compressibility effects are not always negligible[2]. However for many purposes it suffices to assume that density is independent of pressure.

The dependence of the density of seawater on S and T at the surface of the ocean is shown in Fig.9.2. What is actually plotted is the density *anomaly* σ (see Section 7.3),

$$\sigma = \rho - \rho_{_{ref}} \ , \tag{9.2}$$

the difference between the actual density and a reference value $\rho_{ref} = 1000\,\mathrm{kg\,m}^{-3}$. From Fig.9.2 we see that:

1. salty water is more dense than fresh water; warm water is (almost always) less dense than cold water

2. fresh water ($S = 0$) has a maximum density at about 4 °C: fresh water that is colder than this is less dense. This is why ice forms on the top

[2]It is interesting to note that if sea water were really incompressible, sea level would be about 50 m higher than it actually is.

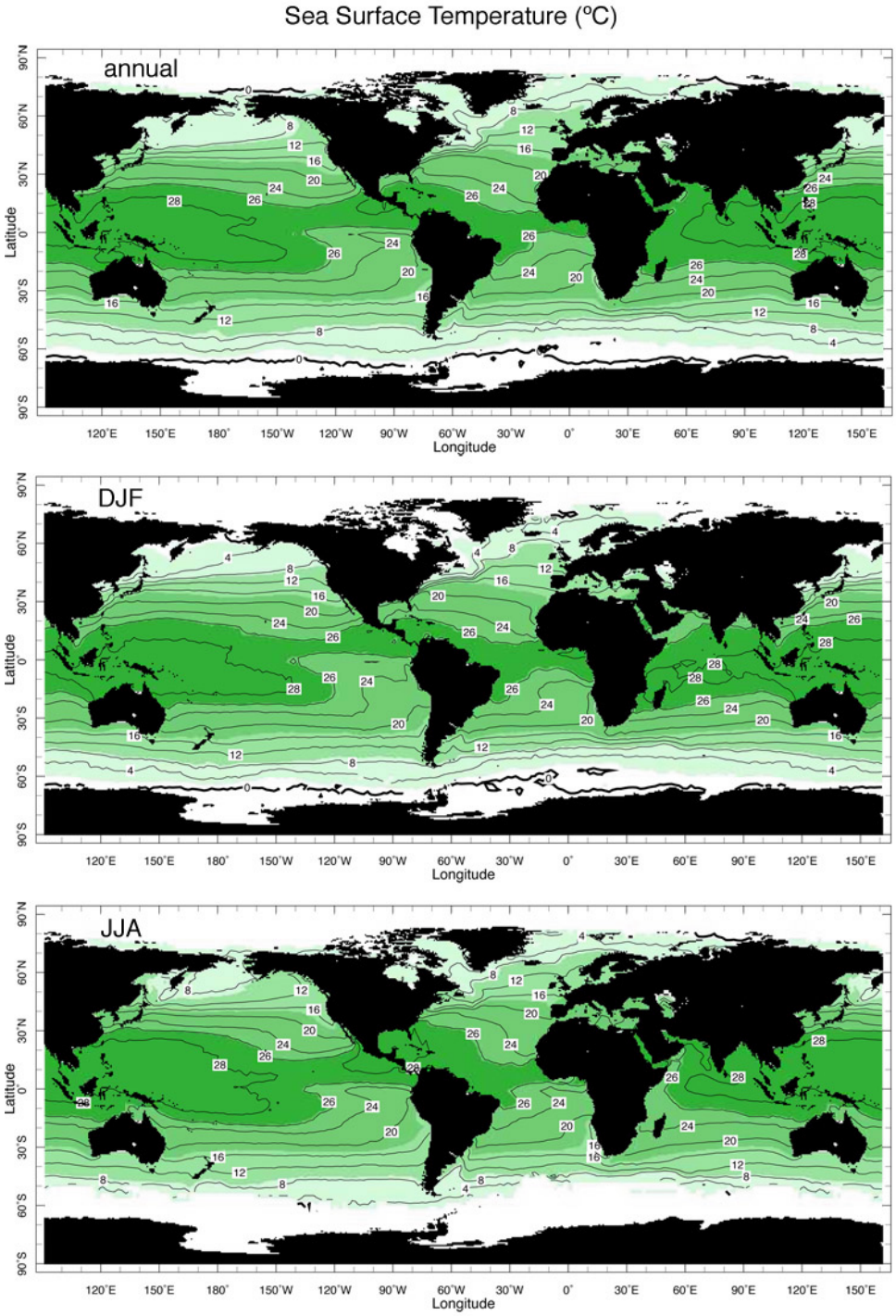

Figure 9.3: Average (a) annual-mean (b) DJF and (c) JJA sea-surface temperature (°C) from the Comprehensive Ocean-Atmosphere Data Set (COADS). Note that there are data void regions in the proximity of ice-covered areas particularly around Antarctica in the southern hemisphere winter. The Antarctic ice edge is farthest north in September and occasionally crosses 60°S.

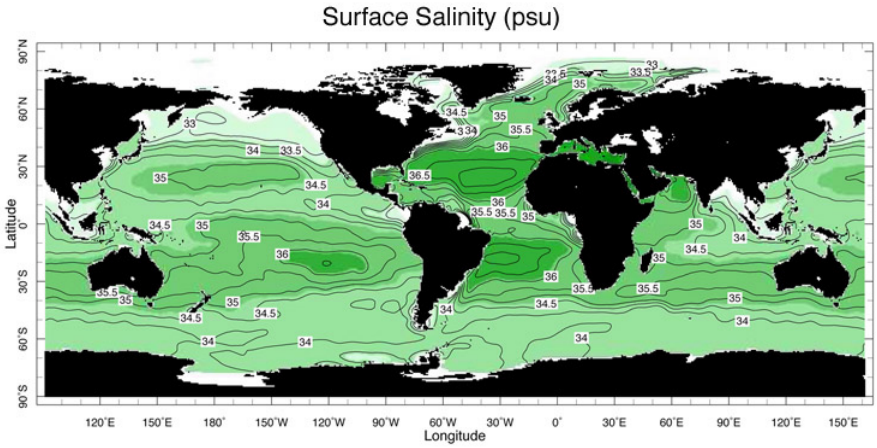

Figure 9.4: The annual mean salinity distribution at the surface of the ocean in psu. Darker green represents salty fluid. Data from Levitus World Ocean Atlas, 1994.

of freshwater lakes: cooling from the surface in winter forms ice rather than denser water.

3. in the (rather narrow) range of temperatures and salinities found in the open ocean (0 to 30 °C and 33-36 psu, see Figs. 9.3 and 9.4), temperature typically influences density more than salinity: at the sea surface σ is typically 26 kg m^{-3} and varies monotonically with temperature.

The thermal expansion coefficient of water, α_T, defined by:

$$\alpha_T = -\frac{1}{\rho_{ref}}\frac{\partial \rho}{\partial T} \ , \tag{9.3}$$

(S and p kept constant) has a typical value of 1×10^{-4} °C^{-1}and is larger at higher temperatures (note how the isopleths of σ in Fig.9.2 slope increasingly upwards with increasing T) and at greater pressures — see Table 9.4.

The dependence of density on salinity is defined by:

$$\beta_S = \frac{1}{\rho_{ref}}\frac{\partial \rho}{\partial S} \tag{9.4}$$

(where T and p is kept constant). As can be seen in Fig.9.2 and Table 9.4, β_S varies very little and has a value close to $7.6 \times 10^{-4}\text{psu}^{-1}$.

It is sometimes useful to approximate the dependence of σ on T, S and p using the following highly simplified equation of state obtained by drawing short lines tangent to the isopleths of σ in Fig.9.2 and writing:

$$\sigma = \sigma_o + \rho_{_{ref}} \left(-\alpha_T \left[T - T_o \right] + \beta_S \left[S - S_o \right] \right) \tag{9.5}$$

where $\sigma_o(T_o, S_o)$ is the density anomaly (at the point T_o and S_o in Fig.9.2), about which we draw the tangent line to compute (small) variations in σ. Note that pressure dependence in the above idealized expression is captured by making $\alpha_T = \alpha_T(p)$ — see Table 9.4. Recall that a simplified form of Eq.(9.5) was used in our discussions of convection of an incompressible fluid in Section 4.2.2.

9.1.4 Temperature, salinity and temperature structure

Here we briefly describe the large-scale distribution of temperature and salinity at the surface of the ocean and its interior. We postpone an attempt at an 'explanation' until Chapters 10 and 11.

Water has an albedo of around 10% (see Table 2.2) depending on surface conditions, and so absorbs solar radiation very efficiently. Not surprisingly sea surface temperatures, plotted in Fig.9.3, are warmest in the tropics (up to almost 30 °C) and coldest (0 °C) in high latitudes. The warmest water — that with a temperature greater than about 29 °C — follows the sun north and south. But there are also large east-west variations, particularly in the tropics, with relatively cool temperatures in the east, and the warmest temperatures west of the International Date Line. This latter region coincides with the location of greatest atmospheric convection (see Fig.4.26), which can become very vigorous when ocean temperatures exceed about 27 °C, an indication of the climatic importance of the tropical Pacific Ocean (to be discussed in Section 12.2). In middle latitudes there are large east-west differences in SST related, as we shall see, to the juxtaposition of equatorward flowing cold boundary currents and poleward flowing warm boundary currents (e.g., in the region of the Gulf Stream in the Atlantic and the Kuroshio in the Pacific). There are also cold regions off California and Africa which are not so obviously related to the advective influence of ocean currents. One also observes strong meridional gradients in SST in the southern ocean

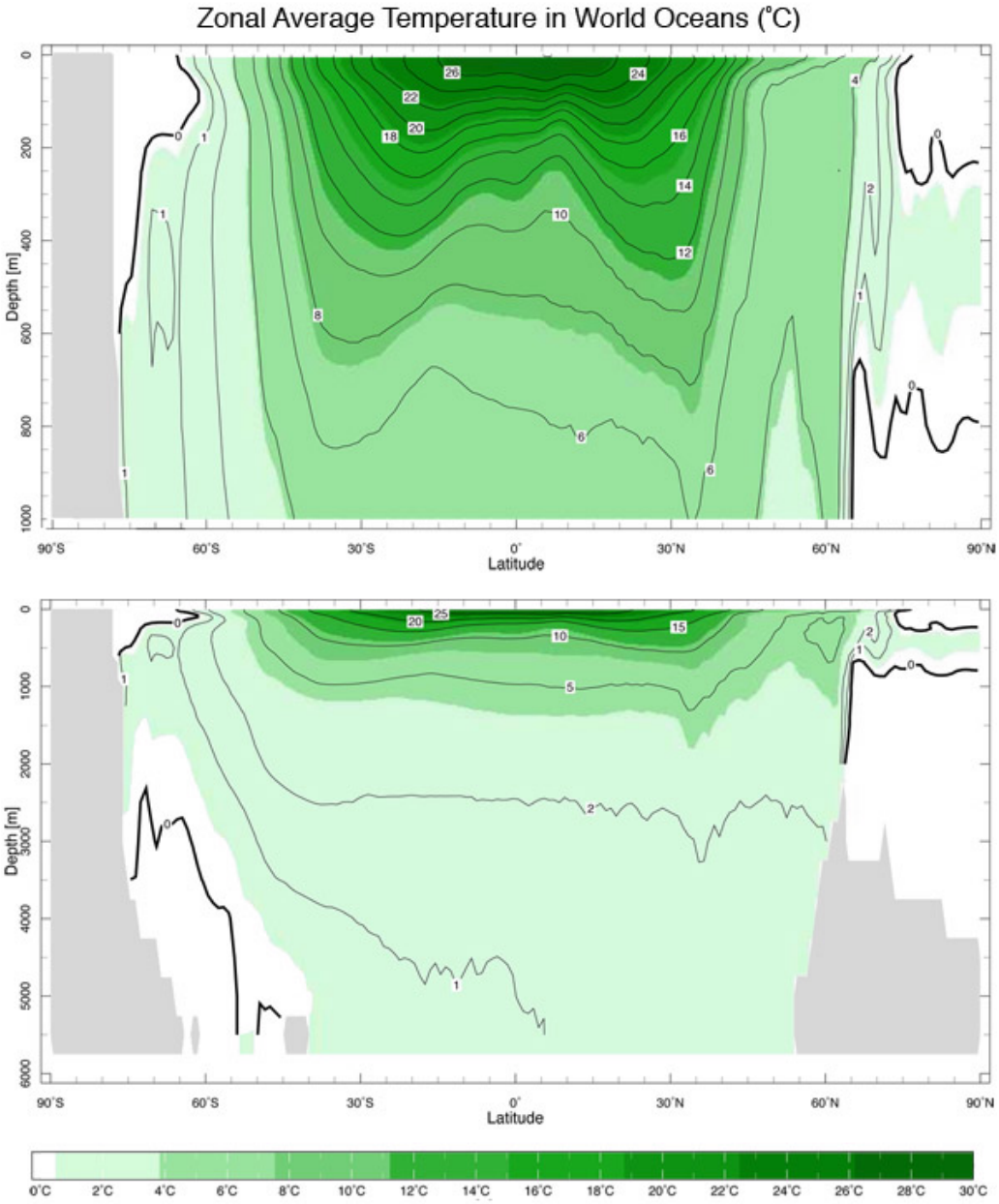

Figure 9.5: Annual-mean cross-section of zonal-average potential temperature (in °C) in the world's oceans: top shows upper 1 km, bottom shows the whole water column. Dark shading represents warm water. Note the variable contour interval in the bottom plot. Data from the Levitus World Ocean Atlas 1994.

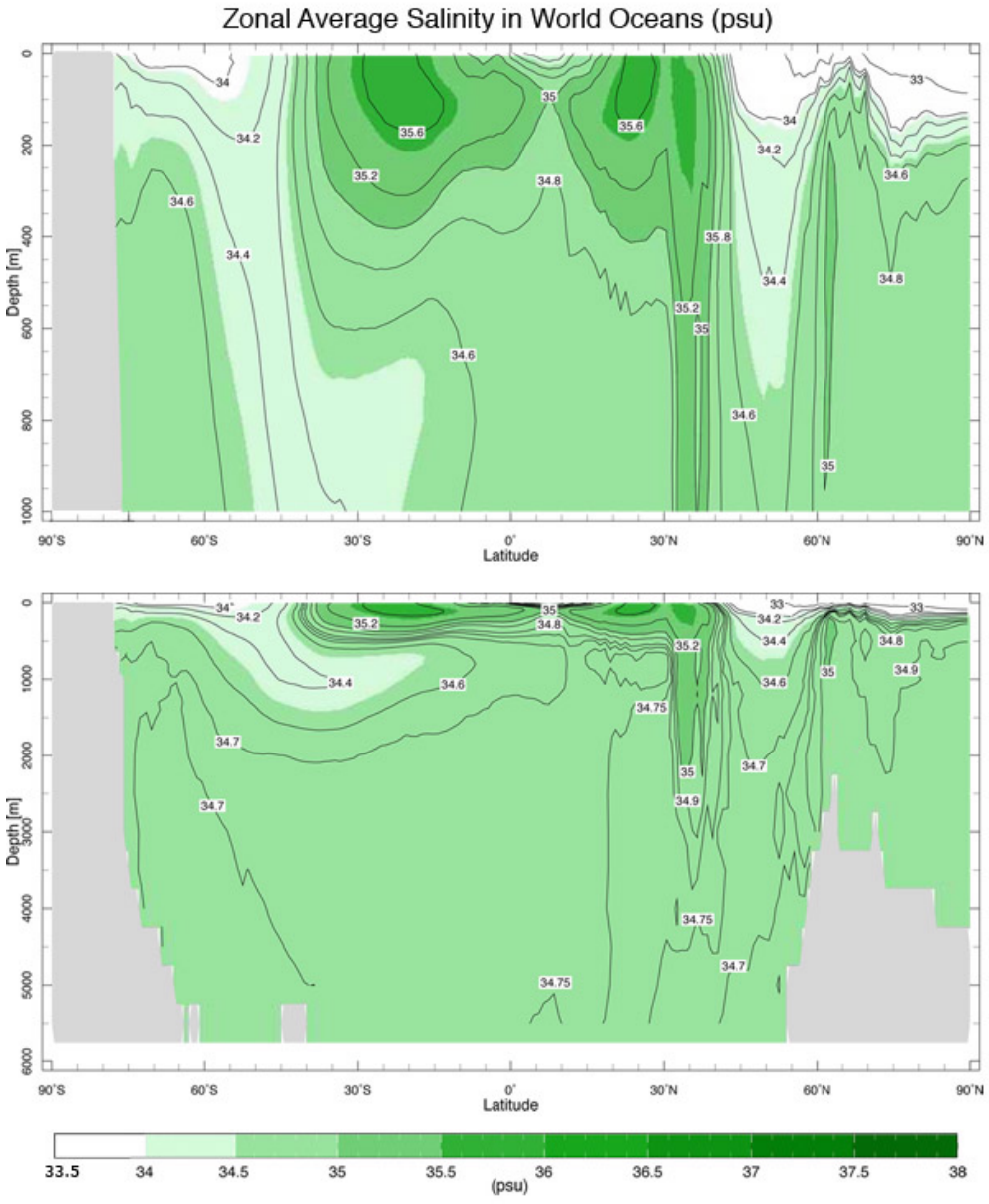

Figure 9.6: Annual-mean cross-section of zonal-average salinity (in psu) in the world's oceans: top shows upper km, bottom shows the whole water column. Darker represents salty water. Data from the Levitus World Ocean Atlas 1994.

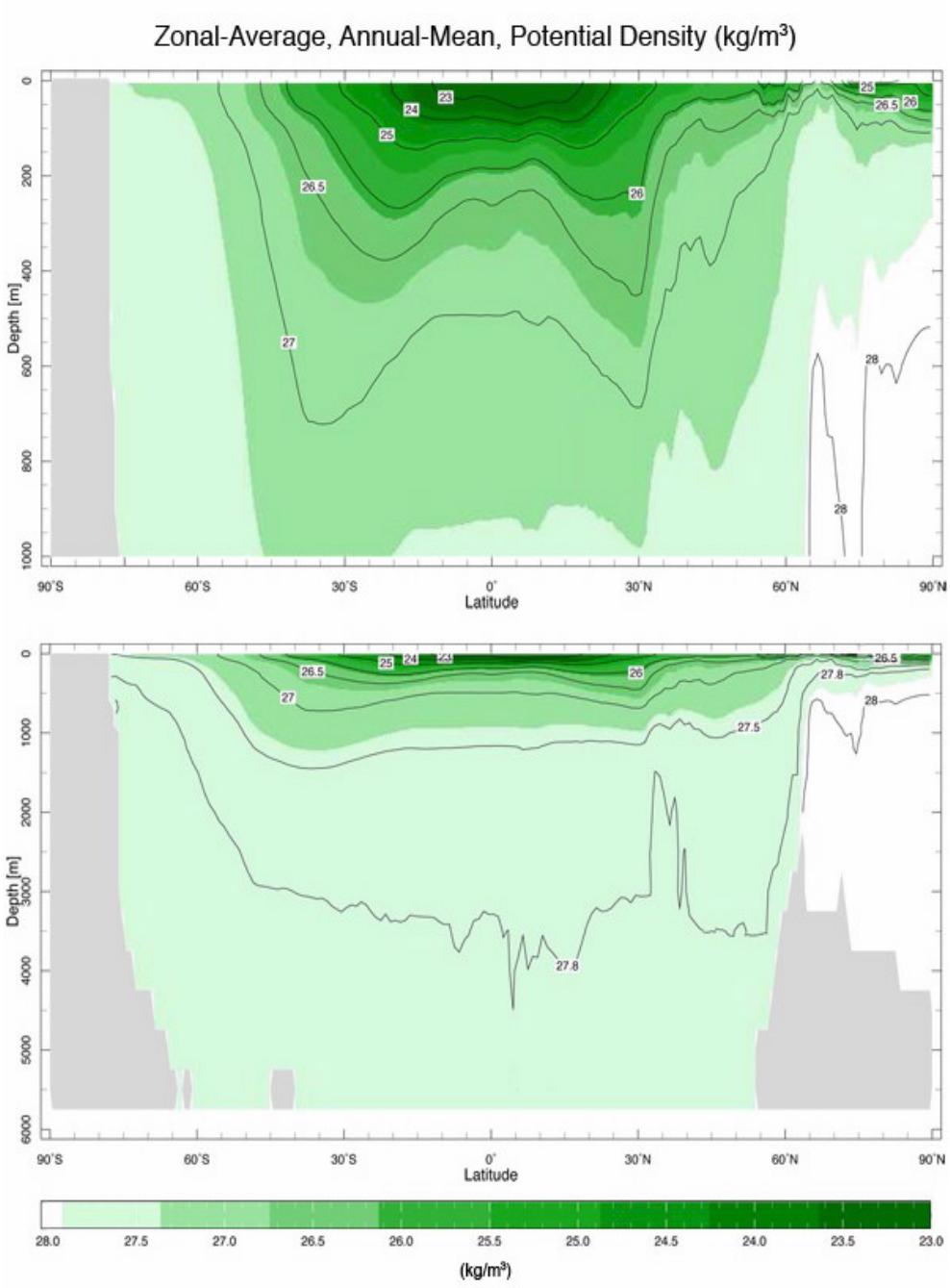

Figure 9.7: Annual-mean cross-section of zonal average potential density anomaly $\sigma = \rho - \rho_{ref}$ (in $\mathrm{kg\,m^{-3}}$) for the world oceans (referenced to the surface): top shows upper 1 km, bottom shows the whole water column. Note that the contour interval is not uniform. Data from the Levitus World Ocean Atlas 1994.

associated with the eastward flowing Antarctic Circumpolar Current. The coldest surface waters are found in the northern North Atlantic Ocean and around Antarctica. As will be discussed in Chapter 11, these are regions of deepest ocean convection where the surface ocean communicates with the abyss.

The annual mean salinity distribution at the surface of the ocean is shown in Fig.9.4. Evaporation from the surface in the subtropics is vigorous and exceeds precipitation; since evaporation removes water, but not salt, the near-surface salinity is elevated here. In high latitudes and near the equator, there is an excess of precipitation over evaporation, so the surface waters are relatively fresh here. High values of salinity (> 38 psu) are found in the Mediterranean and Persian Gulf. Low values of salinity (< 31 psu) are found near melting ice edges and at river outflows. Note that the surface salinity in the Atlantic is higher than that in the Pacific, making Atlantic surface waters more susceptible to convection.

Observed zonal-average mean distributions of T, S, and σ in the interior of the ocean are shown[3] in Figs.9.5, 9.6 and 9.7. Note that the top panel in each of these figures shows a blow-up of the upper 1000 m of the ocean; the bottom panel plots properties over the full ocean depth. The reason for this is that the largest vertical gradients of properties are found near the surface. In the abyss, vertical gradients are weak and horizontal gradients are almost nonexistent; *e.g.*, the deep ocean is everywhere very cold (between 0 and 2 °C) and no more that 1 °C warmer in the tropics than in high latitudes — see Fig.9.5. In the upper kilometer of the ocean, however, shown in the top panels of Figs.9.5, 9.6 and 9.7, there are strong vertical gradients (especially of temperature and density); this is the *thermocline* of the world's oceans having a depth of about 600 m in middle latitudes but shoaling to $100-200$ m in low latitudes. The temperature contrast between high and low latitudes is not surprising; the salinity contrast, as noted above and discussed in Chapter 11, reflects the pattern of evaporation and precipitation. Notice

[3]In fact, what is shown in Figs.9.5 and 9.7 are *potential* temperature and *potential* density, allowing for compressibility effects. Potential temperature, in direct analogy to its definition in a compressible fluid like the atmosphere (Section 4.3.2) is the temperature which a water parcel would have if moved adiabatically to a reference pressure, commonly chosen to be the sea surface. We define potential density as the density a parcel would have when moved adiabatically to a reference pressure. If the reference pressure is the sea surface, we compute the potential temperature of the parcel, and evaluate the density at zero pressure. The measured salinity is used as it has very little pressure dependence.

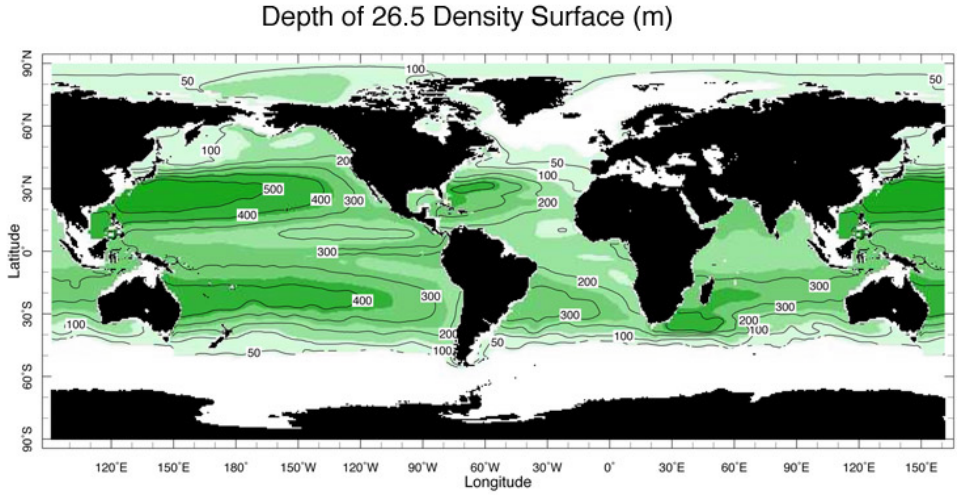

Figure 9.8: Depth in m of the annual-mean $\sigma = 26.5$ kg m^{-3} surface over the global ocean. Note the position of the outcrop — the line along which the σ surface cuts the sea surface — in the North Atlantic and in the southern ocean. Data from the Levitus World Ocean Atlas 1994.

how, particularly around Antarctica, cold surface waters can be less dense than warmer fluid beneath because it is so much fresher. Note also that the contours of temperature, salinity and density anomaly "outcrop" (rise to the surface) in high latitudes, suggesting an important linkage between the high latitude surface waters and the deep ocean.

In summary, the zonal average picture reveals a warm, salty, light lens of fluid in the subtropics of each hemisphere, shoaling on the equatorial and polar flanks, 'floating' on a cold, somewhat fresher abyss. These lenses exist in each ocean basin but exhibit considerable regional characteristics and variability. For example, Fig.9.8 maps the depth of the $\sigma = 26.5$ kg m^{-3} surface over the global ocean; we choose the depth of this surface because, as can be seen in the zonal-average plot, Fig.9.7, it lies roughly in the middle of the thermocline. One can readily observe the geography of the subtropical lenses of light fluid in both the northern and southern hemispheres. Note that the lens is deeper in the Pacific than the Atlantic and outcrops in the Atlantic near 40° N and around the southern ocean.

Fig.9.9 shows a detailed hydrographic section[4] of T and S along (nominally) 30°W in the Atlantic. The thermocline is clearly visible, deep in the subtropics ($\pm 30°$), shallow in equatorial regions and has much more detailed structure than the zonally-averaged view of the thermocline evident in Fig.9.5. The salinity field reveals an interesting layering of subsurface flow which we discuss in more detail in Section 11.2.

9.1.5 The mixed layer and thermocline

At the surface of the ocean there is a well-defined *mixed layer* in direct contact with the overlying atmosphere, stirred by winds and convection, in which properties are relatively uniform in the vertical. The mixed layer depth varies with latitude and season, but is typically $50 - 100\,\mathrm{m}$ deep (see Fig.9.10). Over the bulk of the ocean the mixed layer communicates with the underlying thermocline, except in high latitudes (particularly in the northern North Atlantic and around Antarctica) where it can get very deep ($> 1\,\mathrm{km}$) and thus comes into direct contact with the abyss.

The processes forming the mixed layer are illustrated schematically in Fig.9.11. Radiation entering the ocean surface is absorbed mostly in the top few meters (depending on wavelength; IR is absorbed within a few mm, blue/green light may penetrate to almost 100 m in especially clear water, but is usually attenuated much more rapidly). Heat loss, through IR radiation, sensible heat loss to the atmosphere, and latent heat loss through evaporation (see Chapter 11 for a more detailed discussion), occur at or within a few mm of the surface. The cooling and salinization of the surface water increases its density. Since, in an incompressible fluid, our criterion, Eq.(4.5), for the onset of convection is $\partial\rho/\partial z > 0$, surface buoyancy loss drives convective motions which stir the mixed layer and tend to homogenize its temperature and other properties, just as studied in GFD Lab II in Section 4.2.4. These turbulent motions within the mixed layer may entrain cold water upward

[4] A hydrographic section is a section of T and S as a function of depth, obtained by lowering a CTD (a device that measures Conductivity — hence salinity — Temperature and Depth) from a ship to the bottom of the ocean. It takes of order 1 month to complete a section such as Fig.9.9 and so gives us a snap-shot of the interior T, S structure of the ocean. The average sections shown in, for example, Figs.9.5 and 9.6 are obtained by zonally-averaging hundreds of such sections crisscrossing the ocean. Such zonal-average sections give us a coarse, blurred, but nevertheless instructive view of the meridional structure.

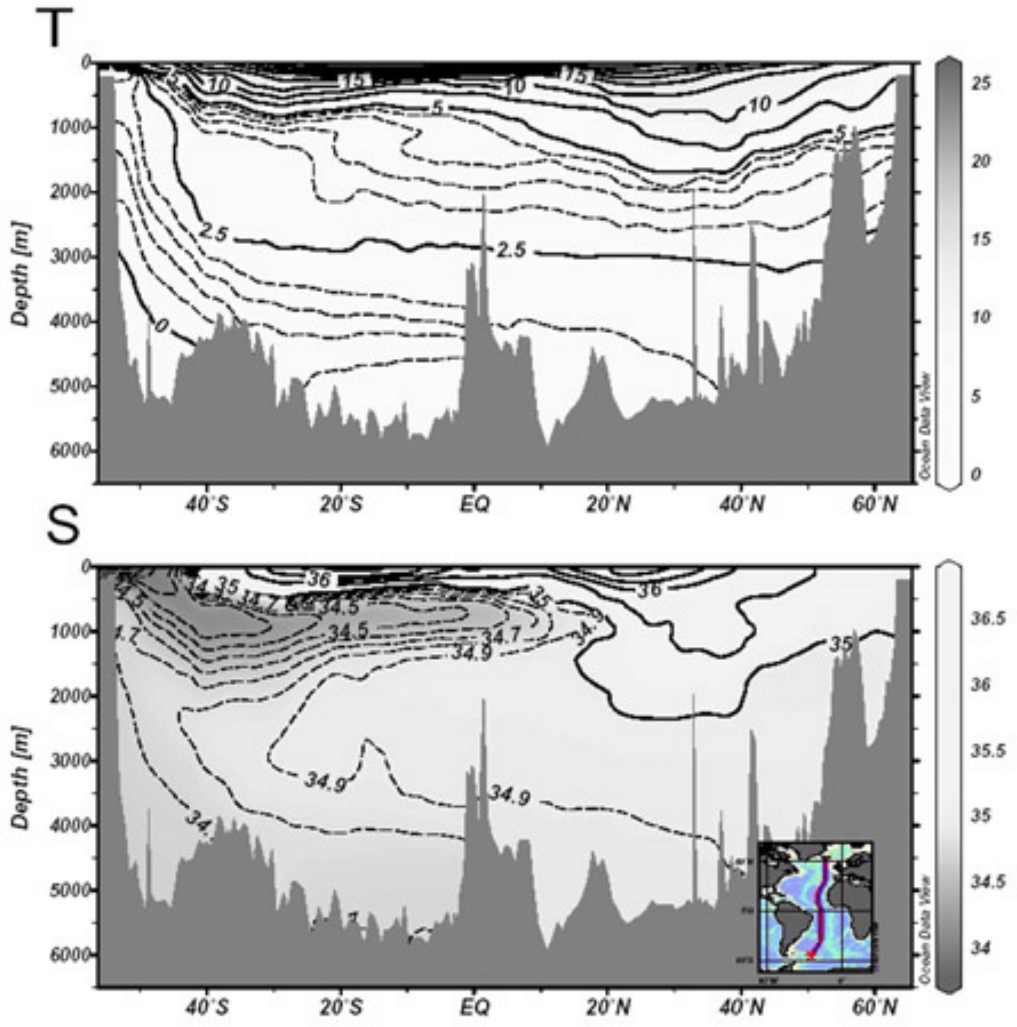

Figure 9.9: Hydrographic section along (roughly) 25°W through the Atlantic Ocean — see inset. Top: Potential temperature contoured every 2.5 °C (solid) and every 0.5 °C (dotted). Bottom: Salinity in psu. Values greater than 35 are contored every 0.5psu (solid): values less than 35 are plotted every 0.1 psu (dotted). Figure produced using Ocean Data View.

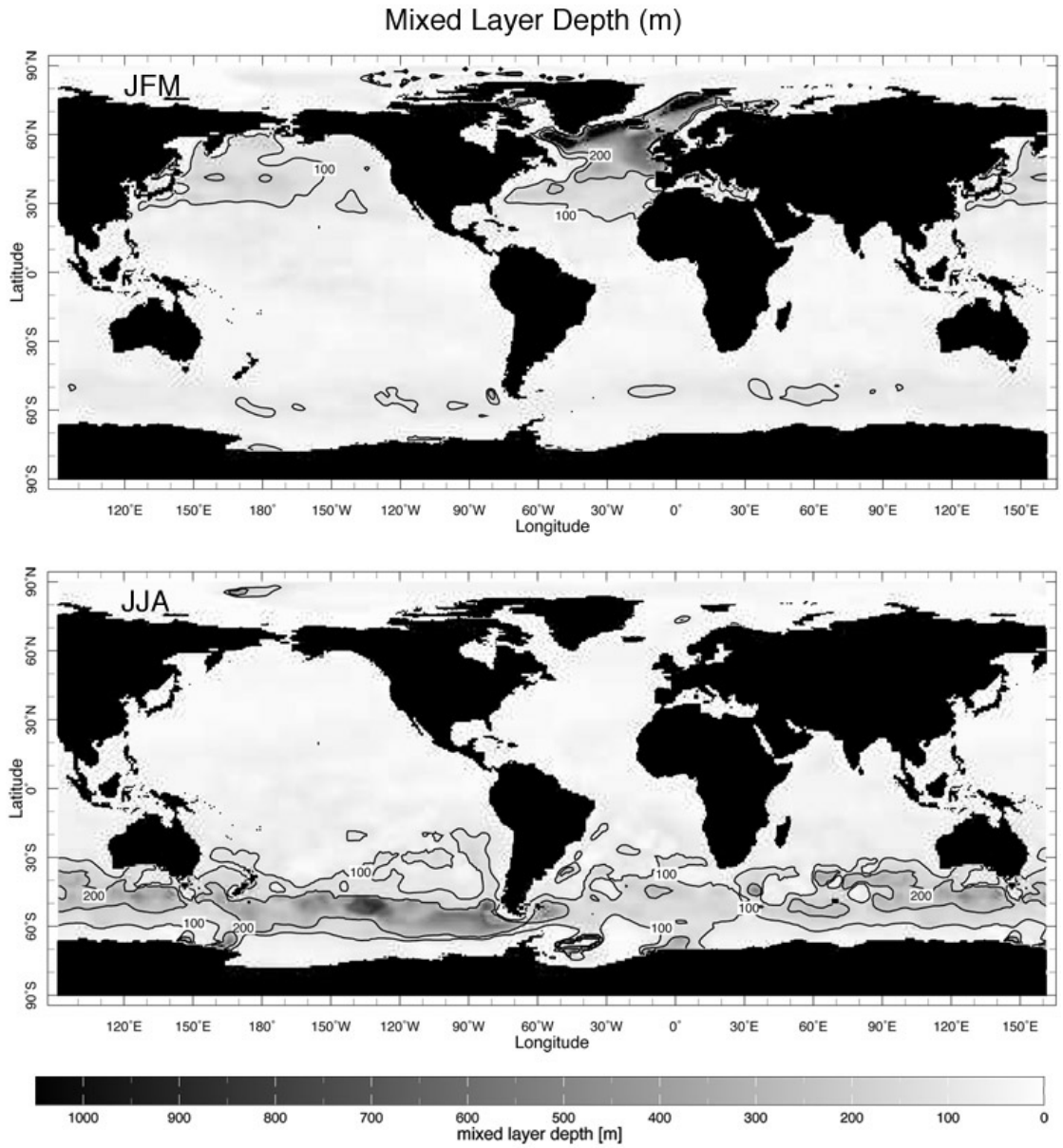

Figure 9.10: Mixed layer depth (in m) in (top) JFM (January, February, March, Northern hemisphere winter) and (bottom) JJA (June, July, August, Southern hemisphere winter). Black contours mark the 100 and 200 m mixed layer depth isopleths. Data from the Levitus World Ocean Atlas 1994.

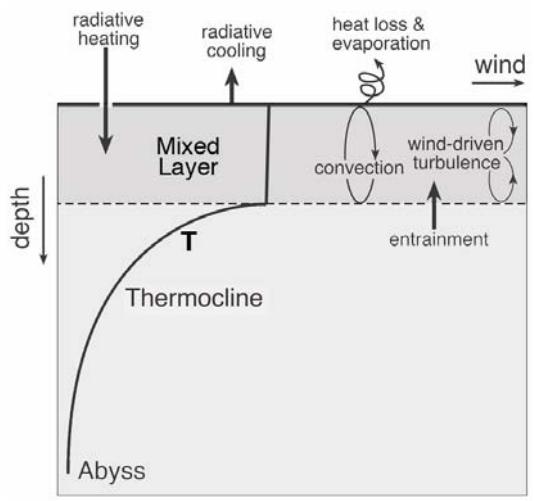

Figure 9.11: A schematic diagram showing processes at work in the mixed layer of the ocean. Note that the vertical scale of the mixed layer relative to the thermocline is greatly exaggerated.

across the mixed layer base. In addition, wind stress at the surface drives turbulent motions within the mixed layer, which mix vertically and entrain fluid from below. Furthermore because the base of the mixed layer slopes (Fig.9.10) horizontal currents can carry properties to and from the mixed layer, in a process known as 'subduction'.

Beneath the mixed layer, T (and S) rapidly change over the depth of the thermocline to match the properties of the relatively homogeneous abyss. Fig.9.12(a) shows the annual mean T and S profile at 50°W, 30°N in the Atlantic Ocean. The thermocline is clearly evident in the upper 1 km of the water column. Since density increases sharply downward across the thermocline, it is very stable, rather like the stratosphere.

We can estimate the buoyancy frequency of the thermocline as follows. Starting from Eq.(4.19) of Section 4.4 and noting that $g\left(\frac{\rho_P-\rho_E}{\rho_P}\right) \simeq -\frac{g}{\rho_E}\frac{d\rho_E}{dz}\Delta = N^2\Delta$, the appropriate definition for our incompressible fluid is:

$$N^2 = -\frac{g}{\rho_{ref}}\frac{d\sigma}{dz} \simeq g\alpha_T\frac{dT}{dz} \tag{9.6}$$

if thermocline density gradients are dominated by temperature gradients and

Eq.(9.5) is used. From Fig.9.12(a), if there is a 15 °C temperature drop across the top 1000 m of the ocean then (using $\alpha_T = 2 \times 10^{-4}\,\mathrm{K}^{-1}$ from Table 9.4) we obtain an N of, in round numbers, $5 \times 10^{-3}\,\mathrm{s}^{-1}$. This implies a period for internal gravity waves in the ocean of $2\pi/N \simeq 20$ min[5], roughly twice that of our estimate in Section 4.4 for atmospheric gravity waves. Indeed T, S surfaces in the interior of the ocean undulate constantly with just this kind of period, excited by winds, flow over topography, tides and myriad other processes. These internal gravity waves are not merely oceanographic noise, in the sense that averaged over many oscillation cycles they disappear. If the waves break, mixing occurs. However the mixing due to internal waves appears to be rather weak in the thermocline (typically eddy diffusivities are $10^{-5}\,\mathrm{m}^2\,\mathrm{s}^{-1}$, albeit two orders of magnitude larger than the molecular diffusivity of water $k = 1.4 \times 10^{-7}\,\mathrm{m}^2\,\mathrm{s}^{-1}$, see Table 9.3), but it can become much larger in the abyss (where N^2 is small), near boundaries and over topography.

An important distinction between the mixed layer and the interior of the ocean is that the former is able to respond rapidly to changes in meteorological forcing. However, the interior, by virtue of its very slow circulation and enormous heat capacity, can only respond very slowly to changing boundary conditions. Thus, for example, the surface mixed layer exhibits diurnal, seasonal and inter-annual variations, whereas the interior ocean evolves on interannual, decadal to centennial (and longer) time scales, the time scale typically increasing with depth. For example, Fig.9.12(b) shows the seasonal cycle of SST and T at 500 m at 50°W, 30°N in the Atlantic. There is no seasonal cycle detectable at 500 m although trends on decadal timescales are observed (not shown).

9.2 The observed mean circulation

The global pattern of mean flow at the surface of the ocean is plotted in Fig.9.13 where the names of the major current systems are also given. The colors separate the circulation patterns into tropical (pink), subtropical (yellow) and subpolar (blue) regimes (inspired by the dynamical discussion to be developed in Chapter 10). Because the detailed patterns are difficult to discern on this global map, regional circulation patterns in the Pacific,

[5]More detailed study shows that $\frac{2\pi}{N}$ is the minimum period for internal waves. More energy is at frequencies closer to f rather than N.

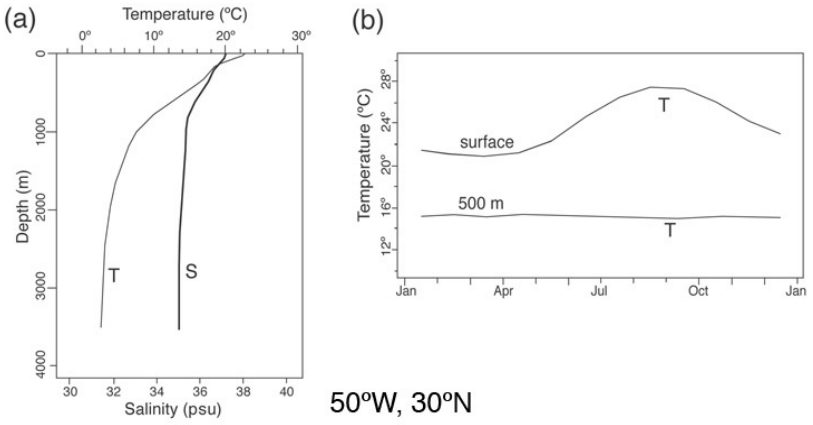

Figure 9.12: (a) Annual mean T and S profile at 50°W, 30°N in the Atlantic Ocean. The thermocline is clearly evident. The T scale is at the top, the S scale at the bottom. (b) The cycle of T at 50°W, 30°N in the Atlantic Ocean in the Levitus monthly mean climatology. The strong seasonal cycle at the surface has vanished at a depth of 500 m. Data from the Levitus World Ocean Atlas 1994.

Atlantic and Indian oceans are also shown in Figs.9.14, 9.15 and 9.16, respectively, with the annual-mean SST superimposed. Note the tiny vector on the bottom right of these plots which represents a current of 10 $\mathrm{cm\,s^{-1}}$, ocean currents are typically 100 times smaller than atmospheric winds. These maps are based on surface drifter data[6] that have been smoothed to aid visual presentation in vector form.

Despite the richness of the structures revealed in these data, on close inspection clear patterns emerge. The flow is dominated by closed circulation patterns known as 'gyres', which are particularly pronounced in the northern hemisphere where all zonal flow is blocked by coasts. In the subtropics of the northern hemisphere there are anticyclonic gyres, known as subtropical gyres (yellow shading in Fig.9.13), with eastward flow in middle latitudes — the North Pacific and North Atlantic Currents — and westward flow in the

[6]Most surface drifters providing these data consist of a spherical surface float tethered to a cylindrical cloth tube hanging below with holes in it centered at a depth of 15 m. Within the float is a radio transmitter allowing it to be located through Doppler ranging by satellite. The drifters can survive for 450 days or so. For a more complete description, see Niiler (2001).

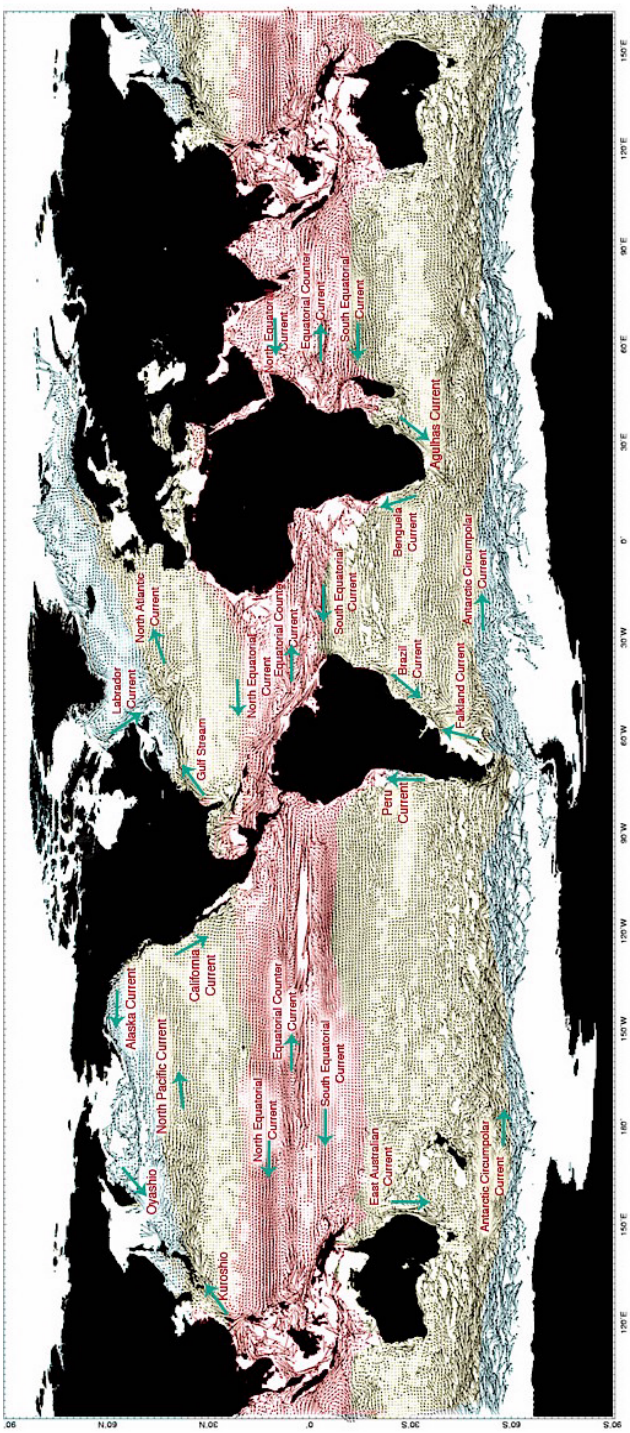

Figure 9.13: Major surface currents observed in the global ocean with the names of key current systems marked. The colors separate the circulation patterns into tropical (pink), subtropical (yellow) and subpolar (blue) regimes based on the pattern of zero wind-curl lines shown in Fig.10.11 (see Section 10.1.3). Data courtesy of Maximenko and Niiler (personal communication, 2003).

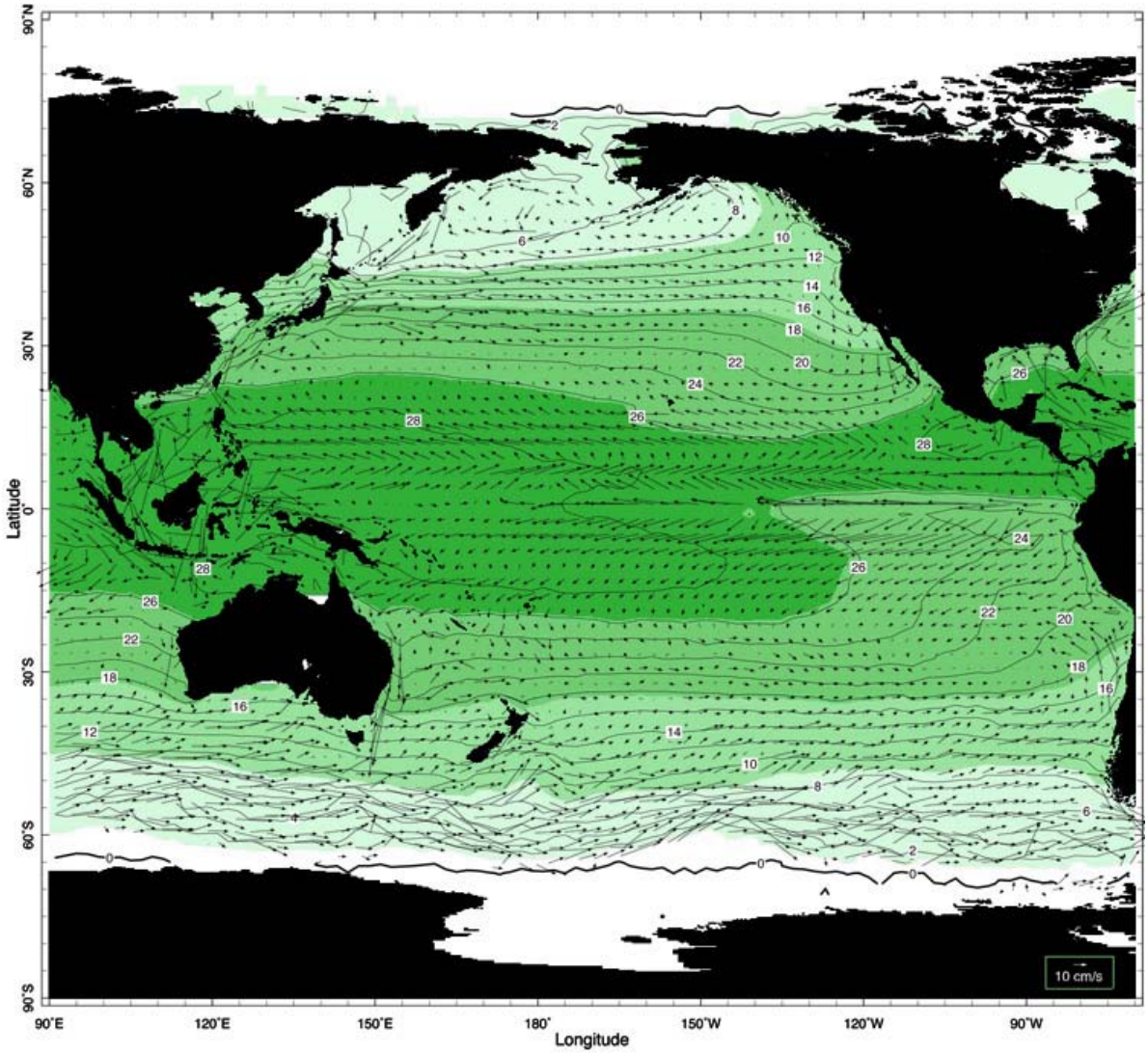

Figure 9.14: Major surface currents observed in the Pacific ocean from surface drifters with annual-mean SST superimposed. The vector at the bottom right represents a current of 10 $\mathrm{cm\,s^{-1}}$. Data courtesy of Maximenko and Niiler (personal communication, 2003).

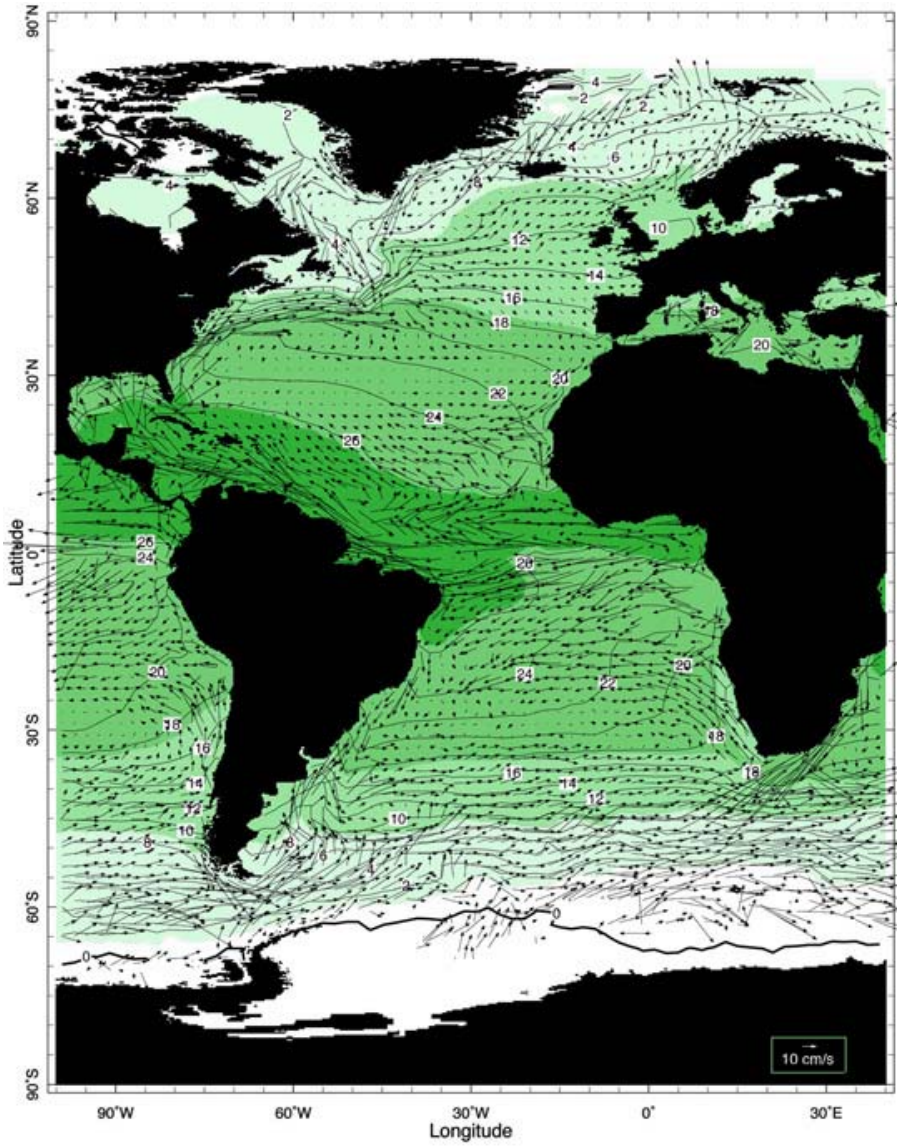

Figure 9.15: Mean surface currents in the Atlantic ocean from surface drifters with annual-mean SST superimposed. The vector at the bottom right represents a current of 10 $\mathrm{cm\,s^{-1}}$. Data courtesy of Maximenko and Niiler (personal communication, 2003).

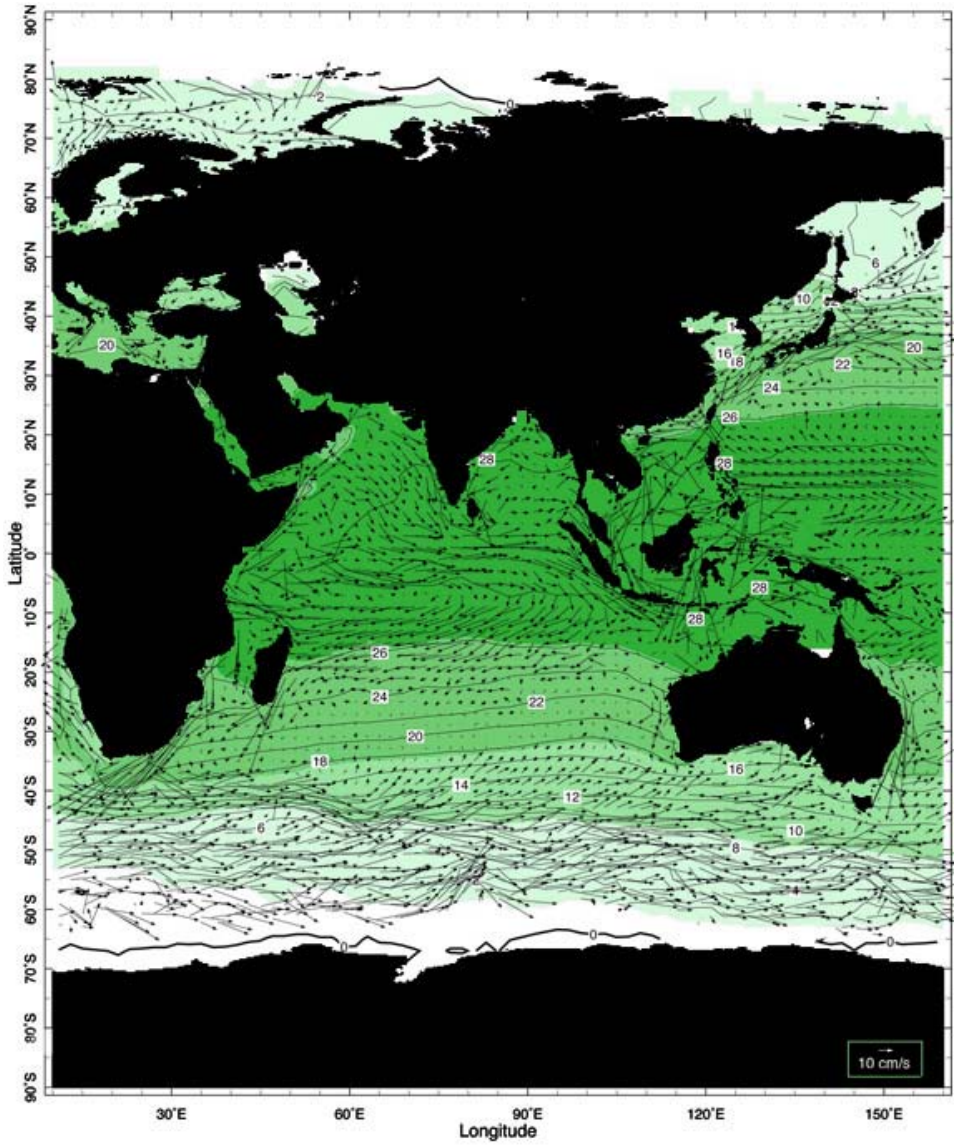

Figure 9.16: Mean surface currents observed in the Indian ocean from surface drifters with annual-mean SST superimposed. The vector at the bottom right represents a current of 10 $\mathrm{cm\,s^{-1}}$. Data courtesy of Maximenko and Niiler (personal communication, 2003).

tropics — the North Equatorial Currents of the Pacific and Atlantic. Typical current speeds in the interior of the gyres are $\lesssim 10\,\mathrm{cm\,s^{-1}}$ (see Fig.9.22top). At the western edge of these subtropical gyres, there are strong, poleward currents reaching speeds $\gtrsim 100\,\mathrm{cm\,s^{-1}}$, the Kuroshio in the N Pacific and the Gulf Stream in the N Atlantic, as is evident in Figs.9.14 and 9.15. These swift currents flow northwards along the coasts from the tropics, turn into the interior at about 40° latitude, and then spread eastward across the ocean basin. This east-west asymmetry is perhaps the most striking aspect of the observed current system — all intense boundary currents are on the western, rather than the eastern, boundaries of ocean gyres. The interior extensions of these boundary currents are evident in the thermal structure at the ocean surface, most obviously in the strong temperature gradients near the western boundaries of the middle-latitude oceans and in the Antarctic Circumpolar Current of the southern hemisphere.

In the polar regions of the north Pacific and Atlantic basins there are cyclonic gyres, known as subpolar gyres (blue shading in Fig.9.13), with southward flowing western boundary currents: the Oyashio Current in the Pacific, the Labrador Current in the Atlantic. Again we observe no intense eastern boundary currents. As discussed earlier, and in more detail in Chapter 11, the northern margin of the subpolar gyres in the Atlantic Ocean — in the Labrador and Greenland Seas — are favoured sites of deep-reaching convection.

In the tropics (pink shading in Fig.9.13) we observe strong zonal flows in each basin, running eastward just north of the equator and counter to the prevailing winds! (see, for example, Fig.7.28, middle panel): the Equatorial Counter Currents very evident in Fig.9.14 have, on either side of them, strong North and South Equatorial Currents flowing westwards. Somewhat weaker meridional temperature gradients are found in the tropics than in higher latitudes but significant zonal temperature gradients exist along the equator. The interaction between the atmosphere and ocean in the tropical Pacific, which leads to variability of the coupled system known as the El-Nino—Southern Oscillation (ENSO) phenomenon, will be addressed in Section 12.2.

In the southern hemisphere, subtropical gyres are also evident[7]. However, on the poleward flanks of the subtropical gyres of the southern ocean, the strong zonal flow of the 'Antarctic Circumpolar Current' (ACC) predominates. Fluid in the ACC can circumnavigate the southern ocean unimpeded by coasts. This is perhaps the ocean current that is most closely analogous to the atmospheric jet stream.

The pattern of mean currents discussed above extend downward in the water column, but the currents become weaker in strength. For example, Fig.9.17 (top) shows currents at a depth of 700 m observed by neutrally buoyant floats[8] in the north Atlantic. We observe a general pattern of currents which is similar to that at the surface (cf. Fig.9.15) but of reduced magnitude. Mean currents in the abyssal ocean are very weak, except in regions of western boundary currents and where flow is channeled by topography. There is significant stirring of the abyss by ocean eddies, however, because the ocean's eddy field typically decays less rapidly with depth than the mean flow.

Before going on to begin our dynamical discussion, we estimate typical timescales associated with the horizontal circulation described above. Tropical surface waters move rather swiftly, reaching mean zonal speeds of 20 cm s^{-1} or more. The Pacific basin is some 14,000 km wide at the Equator,

---

[7] George Deacon, 1906-1984, doyen of British oceanography and father of the 'Institute of Oceanographic Sciences', elucidated the main water masses of the Southern Ocean and their circulation using classical water mass analysis. Deacon's Hydrology of the Southern Ocean, published in 1937, summarized information on the circulation of the southern Atlantic and Southern Ocean and set the standard for future physical oceanographic work.

[8] The sub-surface currents shown in Fig.9.17 were obtained by Profiling Autonomous Lagrangian Current Explorer (PALACE) floats. These are designed to drift at a predetermined depth (700 m in this case) for 10 days or so and then rise to the surface measuring water properties to obtain a temperature and salinity profile. While on the surface, data is transmitted to satellite and the geographic position of the float determined before it returns to depth to repeat the cycle. Each float has battery power for 100 cycles or so. For more details see Davis et al, (2001).

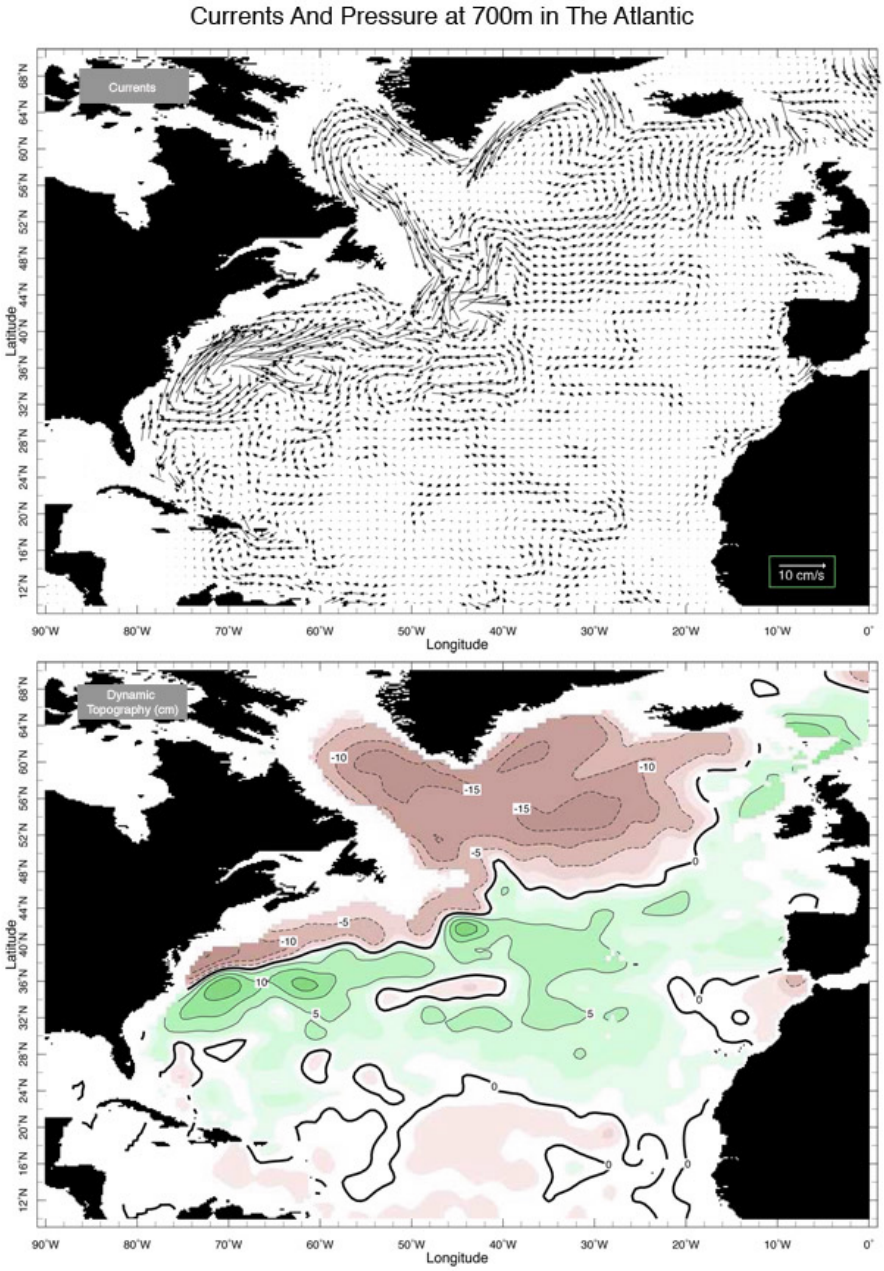

Figure 9.17: (top) Currents at a depth of 700 m in the Atlantic: the arrow at bottom right corresponds to a current of 10 $\mathrm{cm\,s^{-1}}$ (bottom) the associated geostrophic pressure field, expressed as a head of water in cm. Data courtesy of Steve Jayne, WHOI.

yielding a transit time of 2 years or so. Typical zonal surface currents in the ACC are about 30 cm s^{-1} and parcels thus circumnavigate the globe, a distance of some 21,000 km at 55°S, in about 2 years (see Q6 at the end of the Chapter). It takes perhaps 5 years or more for a parcel of water to circulate around the subtropical gyre of the Atlantic Ocean. Timescales of the horizontal circulation increase with depth as the flow decreases in amplitude.

Finally it is important to emphasize that Figs.9.14—9.17 are time-mean circulation patterns. But the ocean is full of time-dependent motions (due to hydrodynamical instabilities and flows driven by variable forcing) so that at any instant the circulation often looks quite different from these mean patterns — as will be discussed in Sections 9.4 and 10.5.

9.3 Inferences from geostrophic and hydrostatic balance

On the large-scale, water obeys the same fluid dynamics as air, so we have already derived the equations we will need: Eq.(6.44) of Chapter 6 applies just as well to the ocean as to the atmosphere. One simplification we can make in application of these equations to the ocean is to recognize that the density varies rather little in the ocean (by only a few %, see Fig.9.2), so we can rewrite the horizontal momentum equations Eq.(6.44)a,b thus (using our local Cartesian coordinate system — see Fig.6.19)

$$\begin{aligned} \frac{Du}{Dt} + \frac{1}{\rho_{ref}}\frac{\partial p}{\partial x} - fv &= \mathcal{F}_x \, ; \\ \frac{Dv}{Dt} + \frac{1}{\rho_{ref}}\frac{\partial p}{\partial y} + fu &= \mathcal{F}_y \, ; \end{aligned} \tag{9.7}$$

without incurring serious error, where ρ_{ref} is our constant reference density. We write the vertical equation, Eq.(6.44)c (hydrostatic balance) in terms of the density anomaly, Eq.(9.2):

$$\frac{\partial p}{\partial z} = -g(\rho_{ref} + \sigma) \, . \tag{9.8}$$

If we neglect the contribution from σ, for a moment, Eq.(9.8) implies that the pressure increases linearly downward from its surface value ($p_s = 10^5$ Pa — one atmosphere) thus,

$$p(z) = p_s - g\rho_{ref}\,(z - \eta) \ , \tag{9.9}$$

where the ocean's surface is at $z = \eta$ and z decreases into the interior of the ocean. This linear variation should be contrasted with the exponential pressure variation of an isothermal compressible atmosphere — see Eq.(3.7) of Chapter 3. The pressure at a depth of, say, 1 km in the ocean is thus about 10^7 Pa or 100 times atmospheric pressure. However, the $g\rho_{ref}z$ part of the pressure field is dynamically inert, because it does not have any horizontal variations. The dynamical part of the hydrostatic pressure is associated with horizontal variations in the free surface height, η, and interior density anomalies, σ, associated with T and S variations and connected to the flow field by geostrophic balance. Finally, it is important to realize that time-mean horizontal variations in surface atmospheric pressure, p_s, turn out to be much less important in Eq.(9.9) than variations in η and σ.[9]

In Section 9.2 we observed that the maximum horizontal current speeds in ocean gyres are found at the surface in the western boundary currents where, instantaneously, they can reach $1\,\mathrm{m\,s^{-1}}$. Elsewhere, in the interior of ocean gyres, the currents are substantially weaker, typically $5 - 10\,\mathrm{cm\ s^{-1}}$, except in the tropical and circumpolar belts. The N-S extent of middle-latitude ocean gyres is typically about 20° latitude ≈ 2000 km (the E-W scale is greater). Thus setting $\mathcal{U} = 0.1\,\mathrm{m\,s^{-1}}$and $L = 2 \times 10^6$ m with $f = 10^{-4}\,\mathrm{s^{-1}}$, we estimate a typical Rossby number, Eq.(7.1), of $R_o = \frac{\mathcal{U}}{fL} \sim 10^{-3}$. This is very small, much smaller, for example, than we found to be typical in the atmosphere where $R_o \sim 10^{-1}$ — see estimates in Section 7.1 and Fig.7.5. Thus the geostrophic and thermal wind approximation is generally excellent for the interior of the ocean away from the equator[10] and away from surface, bottom and side boundary layers. As discussed later in Section 9.3.4, this fact can be exploited to infer ocean currents from hydrographic observations

[9] Suppose, for example, that p_s varies by 10 mbar in 1000 km (corresponding to a stiff surface wind of some $10\,\mathrm{m\,s^{-1}}$ in middle latitudes — see, e.g., Fig.7.25) then the surface geostrophic ocean current required to balance this surface pressure gradient is a factor $\frac{\rho_{atoms}}{\rho_{ocean}} \sim \frac{1}{1000}$ times smaller, or 1 $\mathrm{cm\,s^{-1}}$, small relative to observed surface ocean currents. Mean surface atmospheric pressure gradients are typically considerably smaller than assumed in this estimate — see Fig.7.27.

[10] Our estimate of R_o is applicable to the gyre as a whole. Within the western boundary currents, a more relevant estimate is $U_{bdy}/f\Delta$, where Δ is the width of the boundary current and U_{bdy} is its speed. If $\Delta \sim 100$ km and U_{bdy} reaches $2\,\mathrm{m\,s^{-1}}$, then the Rossby number within these boundary currents can approach, and indeed exceed, unity.

of T and S.

Thus away from (surface, bottom, and side) boundary layers, the geostrophic equations derived in Chapter 7 will be valid: Eqs.(7.3) and (7.4) with, as in Eq.(9.7), ρ_{ref} substituted for ρ. The associated thermal wind equation, Eqs.(7.16) and (7.17), will also apply.

Using Eq.(7.16) one can immediately infer the sense of the thermal wind shear from the σ field shown in, for example, Fig.9.7: $\frac{\partial u}{\partial z} > 0$ where σ increases moving northward in the northern hemisphere ($f > 0$), implying that u at the surface is directed eastward in these regions if abyssal currents are weak. Inspection of Fig.9.7 suggests that $\frac{\partial u}{\partial z}$and the surface u are positive (negative) poleward (equatorward) of 25°N, more or less as observed in Fig.9.14 and 9.15. Moreover, Eq.(7.16) suggests a mean surface geostrophic flow of magnitude:

$$u_{\text{surface}} \sim \frac{g}{f\rho_{ref}} \frac{H\Delta\sigma}{L} \sim 8 \text{ cm s}^{-1}$$

if $\Delta\sigma \sim 1.5\,\text{kg m}^{-3}$ is the change in σ between, say, 20°N and 40°N, a distance $L \sim 2000\,\text{km}$, in the top $H \sim 1000\,\text{m}$ of the ocean seen in Fig.9.7. This is in good accord with direct observations shown, for example, from surface drifters in Fig.9.14.

9.3.1 Ocean surface structure and geostrophic flow

Near-surface geostrophic flow

To the extent that the surface currents shown in Fig.9.14 to 9.16 are in geostrophic balance there must be a pressure gradient force balancing Coriolis forces acting on them. Consider, for example, the eastward flowing Gulf Stream of the Atlantic evident in Fig.9.15. In order to balance the southward-directed Coriolis force acting on it, there must be a pressure gradient force directed northward. This is provided by a tilt in the free surface of the ocean: we shall see that the sea surface is higher[11] to the south of the Gulf Stream

[11] Here 'high' means measured relative to the position that the ocean surface would take up if there were no surface geostrophic flow. This equipotential reference surface is the 'geoid' which is everywhere perpendicular to the local plumb line. Recall that the 'geoid' of our rotating tank of water considered in Section 6.6 is the parabolic surface shown in Fig.6.11. We saw in Fig.6.18 that the geoid surface of the rotating earth approximates a reference ellipsoid. Geoid height variations about this reference ellipsoid are of the order of $\pm 100\,\text{m}$, 100 times larger than height variations associated with geostrophic flow.

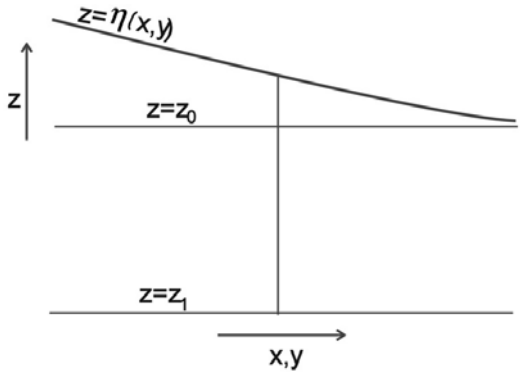

Figure 9.18: The height of the free surface of the ocean is $z = \eta(x, y)$. The depths of two reference horizontal surfaces, one near the surface and one at depth is given by $z = z_o$ and $z = z_1$ respectively.

than to the north of it.

Consider Fig.9.18. Integrating the hydrostatic relation, Eq.(3.3), from some horizontal surface at constant z up to the free surface at $z = \eta$ (where $p = p_s$, atmospheric pressure) we obtain:

$$p(z) = p_s + \int_z^\eta g\rho \, dz \;\; = p_s + g \, \langle \rho \rangle \, (\eta - z) \;\; , \tag{9.10}$$

where $\langle \rho \rangle = \frac{1}{(\eta - z)} \int_z^\eta g\rho \, dz$ is the mean density in the water column of depth $\eta - z$. If we are interested in the near-surface region ($z = z_0$, say, in Fig.9.18), fractional variations in column depth are much greater than those of density, so we can neglect the latter, setting $\rho = \rho_{ref}$ in Eq.(9.10) and leaving

$$p(z_0) = p_s + g\rho_{ref} \, (\eta - z_0) \;\; .$$

We see that horizontal variations in pressure in the near-surface region thus depend on variations in atmospheric pressure and in free-surface height. Since here we are interested in the mean ocean circulation, we neglect day-to-day variations of atmospheric pressure and equate horizontal components of the near-surface pressure gradient with gradients in surface elevation: $\left(\frac{\partial p}{\partial x}, \frac{\partial p}{\partial y} \right) = g\rho_{ref} \left(\frac{\partial \eta}{\partial x}, \frac{\partial \eta}{\partial y} \right)$. Thus, the geostrophic flow just beneath the surface is, from

Eq.(7.4), $(u_{g_{\rm surface}}, v_{g_{\rm surface}}) = \frac{g}{f}\left(-\frac{\partial\eta}{\partial y}, \frac{\partial\eta}{\partial x}\right)$ or, in vector form

$$\mathbf{u}_{g_{\rm surface}} = \frac{g}{f}\widehat{\mathbf{z}} \times \nabla\eta \tag{9.11}$$

Note how Eq.(9.11) exactly parallels the equivalent relationship Eq.(7.7) for geostrophic flow on an atmospheric pressure surface.

In Section 7.1.1 we saw that geostrophic winds of $15\,\mathrm{m\,s^{-1}}$ were associated with tilts of pressure surfaces by about 800 m over a distance of 5000 km. But because oceanic flow is weaker than atmospheric flow, we expect to see much gentler tilts of pressure surfaces in the ocean. We can estimate the size of η variations by making use of Eq.(9.11) along with observations of surface currents: if U is the eastward speed of the surface current, then η must drop by an amount $\Delta\eta$ in a distance L given by:

$$\Delta\eta = \frac{fLU}{g}$$

or 1 m in 1000 km if $U = 10^{-1}\,\mathrm{m\,s^{-1}}$and $f = 10^{-4}\,\mathrm{s^{-1}}$. Can we see evidence of this in the observations?

Observations of surface elevation

Maps of the height of the sea surface, η, give us the same information as do maps of the height of atmospheric pressure surfaces (and, of course, because p_s variations are so slight, the ocean surface is — to a very good approximation — a surface of constant pressure). If we could observe the η field of the ocean then, just as in the use of geopotential height maps in synoptic meteorology, we could deduce the surface geostrophic flow in the ocean. Amazingly, variations in ocean topography, even though only a few centimeters to a meter in magnitude, can indeed be measured from satellite altimeters and are mapped routinely over the globe every week or so. Orbiting at a height of about 1000 km above the Earth's surface, altimeters measure their height above the sea surface to a precision of $1 - 2\,\mathrm{cm}$. And, tracked by lasers, their distance from the center of the earth can also be determined to high accuracy, permitting η to be found by subtraction.

The 10 y-mean surface elevation (*relative* to the mean "geoid") is shown in Fig.9.19. Consistent with Fig.9.14 and 9.15, the highest elevations are in the anticyclonic subtropical gyres (where the surface is about 40 cm higher

than near the eastern boundary at the same latitude), and there are strong gradients of height at the western boundary currents and near the circumpolar current of the Southern Ocean, where surface height changes by about 1 m across these currents.

9.3.2 Geostrophic flow at depth

At depths much greater than variations of η (at $z = z_1$, say, in Fig.9.18), we can no longer neglect variations of density in Eq.(9.10) compared with those of column depth. Again neglecting atmospheric pressure variations, horizontal pressure variations at depth are therefore given by, using Eq.(9.10),

$$\widehat{\mathbf{z}} \times \nabla p = g \langle \rho \rangle \ \widehat{\mathbf{z}} \times \nabla \eta + g(\eta - z) \, \widehat{\mathbf{z}} \times \nabla \langle \rho \rangle \ .$$

Thus the deep water geostrophic flow is given by

$$\begin{aligned} \mathbf{u} &= \frac{1}{f \rho_{ref}} \widehat{\mathbf{z}} \times \nabla p \\ &= \frac{g}{f \rho_{ref}} \left[\langle \rho \rangle \ \widehat{\mathbf{z}} \times \nabla \eta + (\eta - z) \, \widehat{\mathbf{z}} \times \nabla \langle \rho \rangle \right] \\ &\simeq \frac{g}{f} \widehat{\mathbf{z}} \times \nabla \eta + \frac{g(\eta - z)}{f \rho_{ref}} \widehat{\mathbf{z}} \times \nabla \langle \rho \rangle \ , \end{aligned} \tag{9.12}$$

since we can approximate $\langle \rho \rangle \simeq \rho_{ref}$ in the first term because we are not taking its gradient. We see that $\mathbf{u}$ has two contributions: that associated with free-surface height variations, and that associated with interior ocean density gradients. Note that if the ocean density were to be uniform, the second term would vanish and the deep-water geostrophic flow would be the same as that at the surface: *geostrophic flow in an ocean of uniform density is independent of depth*. This, of course, is a manifestation of the Taylor-Proudman theorem, discussed at length in Section 7.2. However, observed currents and pressure gradients at depth are smaller than at the surface (cf. Fig.9.15 and 9.17) suggesting that the two terms on the rhs of Eq.(9.12) tend to balance one-another.

The second term in Eq.(9.12) is the "thermal wind" term (cf. Section 7.3) telling us that $\mathbf{u}$ will vary with depth if there are horizontal gradients of density. Thus the presence of horizontal variations in surface height, manifested in surface geostrophic currents given by Eq.(9.11), does not guarantee

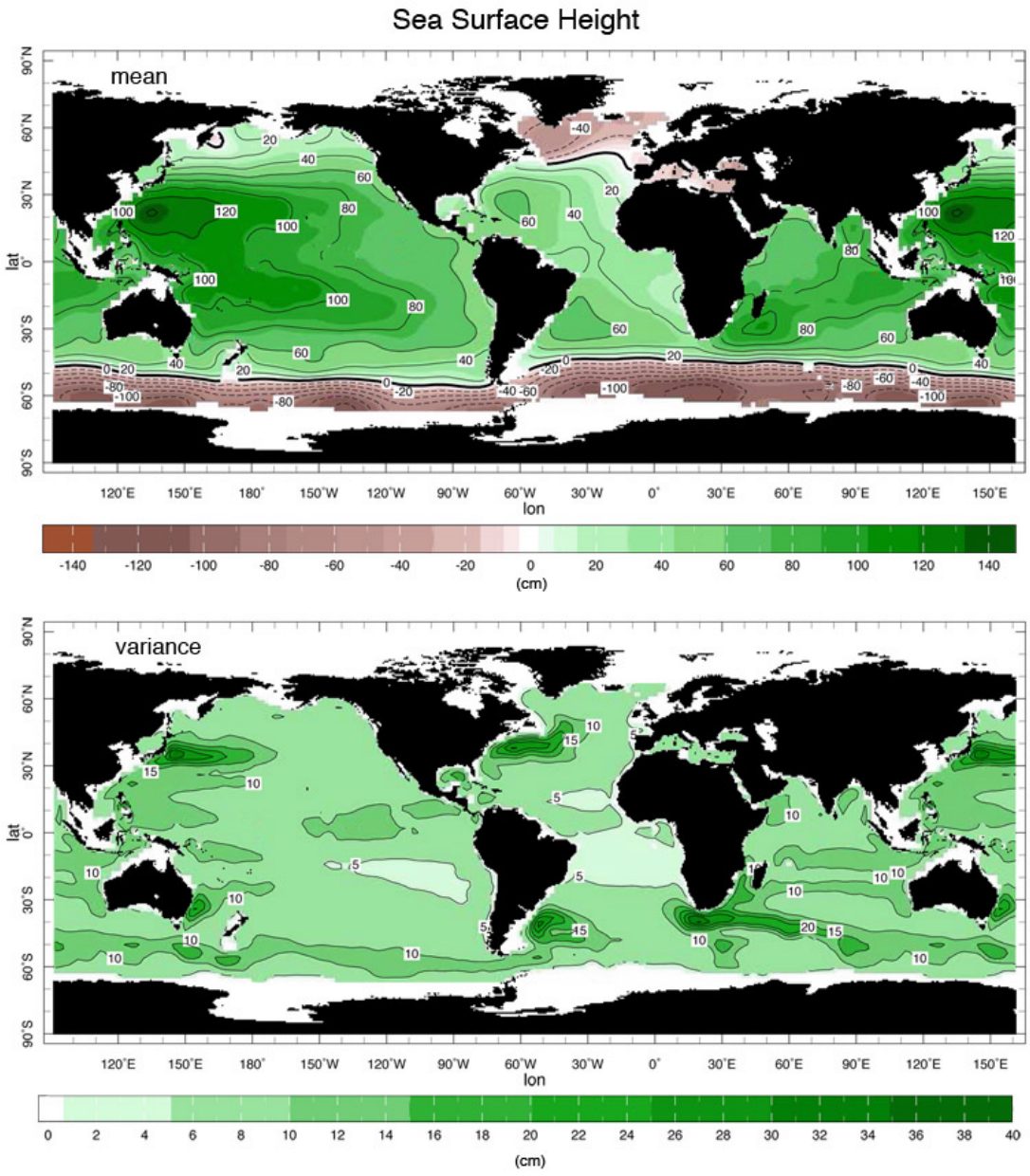

Figure 9.19: (Top) The 10-year mean height of the sea surface relative to the geoid, $\overline{\eta}$, (contoured every 20 cm) as measured by satellite altimeter. The pressure gradient force associated with the tilted free surface is balanced by Coriolis forces acting on the geostrophic flow of the ocean at the surface. Note that the equatorial current systems very evident in the drifter data — Figs. 9.14 and 9.22 — are only hinted at in the sea surface height. Near the equator, where f is small, geostrophic balance no longer holds. (bottom) The variance of the sea surface height, $\sigma_\eta = \sqrt{\overline{\eta'^2}}$, Eq.(9.17), contoured every 5 cm.

a geostrophic flow at depth. Indeed, as already noted, the flow becomes much weaker at depth.

How much would interior density surfaces need to tilt to cancel out deep pressure gradients and hence geostrophic flow? If $\mathbf{u} \longrightarrow 0$ in Eq.(9.12) then, at depth $z = -H$ (assuming $H >> \eta$),

$$\frac{H}{\rho_{ref}} |\nabla \langle \rho \rangle| \approx |\nabla \eta| \ , \tag{9.13}$$

or, dividing through by N^2, Eq.(9.6), we find that the slope of "isopycnals" — interior density surfaces — must be related to the slope of the free surface by:

$$|\text{isopycnal slope}| \approx \frac{g}{N^2 H} \times |\text{free surface slope}|$$

Using our estimate of N^2 in Section 9.1.5, and rearranging, we find that $\frac{g}{N^2 H} \approx 400$ if we assume that $H = 1\,\text{km}$. Thus we see that for every meter the free surface tilts up, density surfaces must tilt down by around 400 m if deep pressure gradients, and hence deep geostrophic flows, are to be cancelled out. But this is just what we observe in, for example, Fig.9.5. In those regions where the sea surface is high — over the subtropical gyres (see Fig.9.19) — density surfaces bow down into the interior (see Fig.9.8). In the subpolar gyre (where the sea surface is depressed) we observe density surfaces bowing up toward the surface. It is these horizontal density gradients interior to the ocean that 'buffer out' horizontal gradients in pressure associated with the tilt of the free surface; in the time-mean, the second term in Eq.(9.12) does indeed tend to cancel out the first. This is illustrated schematically in Fig.9.20.

9.3.3 Steric effects

A major contribution to the spatial variations in the height of the ocean surface shown in Fig.9.19, is simply the expansion (contraction) of water columns that are warm (cold) relative to their surroundings. Note that the sea surface is high over the subtropical gyres which are warm, and low over the subpolar gyres, and around Antarctica, which are relatively cold. Similarly, salty columns of water are shorter than fresh columns, all else being equal. This expansion/contraction of water columns due to T and S anomalies is

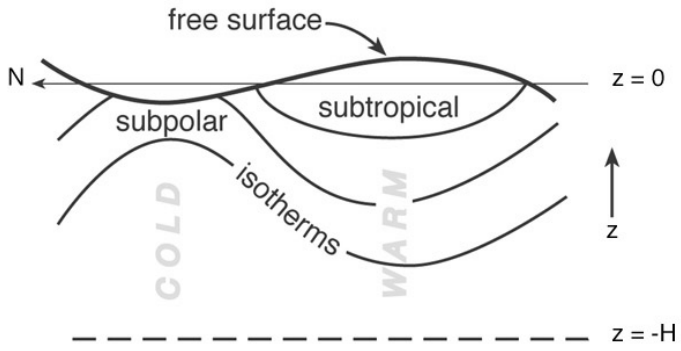

Figure 9.20: Warm subtropical columns of fluid expand relative to colder polar columns. Thus the sea surface (measured relative to the geoid) is higher, by about 1 m, in the subtropics than the pole, and is thus greatly exaggerated in this schematic. Pressure gradients associated with the sea-surface tilt are largely compensated by vertical thermocline undulations, of about 400 m, ensuring that abyssal pressure gradients are much weaker than those at the surface.

known as the 'steric effect'. We can estimate its magnitude from Eq.(9.13) as follows:

$$\frac{\Delta\eta}{H} \simeq (\alpha_T \langle T - T_o \rangle - \beta_S \langle S - S_o \rangle) \tag{9.14}$$

where, as before, the angle brackets denote $\langle () \rangle = \frac{1}{(H+\eta)} \int_{-H}^{\eta} () \; dz$ and Eq.(9.5) has been used. From Fig.9.5 we estimate that $\langle T - T_o \rangle \simeq 10\,^\circ\mathrm{C}$ over the top km of the warm water lens of the subtropical gyres and, from Fig.9.6, $\langle S - S_o \rangle \simeq 0.5$psu. Thus if (see Table 9.4) $\alpha_T = 2 \times 10^{-4}\,^\circ\mathrm{C}^{-1}$ and $\beta_S = 7.6 \times 10^{-4}\mathrm{psu}^{-1}$ we find that:

$$\frac{\Delta\eta}{H} \simeq \left(\underbrace{2}_{temp} + \underbrace{-0.38}_{salt} \right) \times 10^{-3}$$

We see that over the top km or so of the column, height variations due to salt are more than offset by the 2 m of expansion due to the warmth of the surface lens. These estimates of gradients in surface elevation are broadly consistent with Fig.9.19 (top).

9.3.4 The dynamic method

The thermal wind relation, Eq.(7.17), is the key theoretical relationship of observational oceanography, providing a method by which observations of T and S as a function of depth can be used to infer ocean currents.[12] Let us vertically integrate, for example, Eq.(7.16)a from level z to z_1 — see Fig.9.18 — to obtain:

$$u_g(z) - u_g(z_1) = \frac{g}{f}\int_{z_1}^{z} \frac{1}{\rho_{ref}}\frac{\partial \sigma}{\partial y} dz = \frac{g}{f}\frac{\partial \mathcal{D}}{\partial y} \tag{9.15}$$

where

$$\mathcal{D} = \int_{z_1}^{z} \frac{\sigma}{\rho_{ref}} dz \tag{9.16}$$

is known as the 'dynamic height'.

Given observations of T and S with depth (for convenience pressure is typically used as the vertical coordinate) from a hydrographic section such as Fig.9.21, we compute σ from our equation of state of seawater, Eq.(9.1), and then vertically integrate to obtain $\mathcal{D}$ from Eq.(9.16). The geostrophic flow u_g at any height relative to the geostrophic current at level $u_g(z_1)$ is then obtained from Eq.(9.15) by taking horizontal derivatives. This is called the 'dynamic method'. Note, however, that it only enables one to determine geostrophic velocities relative to some reference level. If we assume, or choose z_1 to be sufficiently deep that, given the general decrease of flow with depth,

[12] Georg Wust (1890-1975), a Berliner who dedicated his life to marine research, was the first to systematically map the vertical property distribution and circulation of the ocean. In 1924, using the Florida Current as an example, Wust apparently confirmed that the geostrophic shear measured by current meters were broadly consistent with those calculated from the pressure field using geostrophic balance and the dynamic method.

$u_g(z_1)$ is far smaller than $u_g(z)$, then we can proceed. Indeed, upper ocean velocities are insensitive to the assumption of a deep 'level of no motion'. However, deep water *transport* calculations, $\int u_g dz$, are extremely sensitive to this assumption that is rarely true. Alternatively we can make use of altimetric measurements or surface drifters, such as those shown in Figs.9.13 and 9.19, choose the sea surface as our level of known geostrophic flow and integrate downwards.

As an example of the dynamic method we show $\mathcal{D}$ in Fig.9.21(bottom) cutting across the Gulf Stream computed relative to a depth of 2 km. It increases from zero at 2 km to of order 1 m at the surface. Taking horizontal derivatives and using Eq.(9.15), we deduce that $u_g(z)$ relative to 2 km is $\simeq \frac{9.81\,\mathrm{m\,s^{-2}}}{2\Omega \sin 52^\circ\,\mathrm{s^{-1}}} \frac{1\,\mathrm{m}}{100\times 10^3\,\mathrm{m}} = 0.85\,\mathrm{m\,s^{-1}}$. This is a swift current but typical of Gulf Stream speeds which, instantaneously, can reach up to $1-2\,\mathrm{m\,s^{-1}}$.

9.4 Ocean eddies

9.4.1 Observations of ocean eddies

Figs.9.14 to 9.16 show currents averaged over many (about 20) years of observations. However, just as in the atmosphere (in fact, even more so) the picture we have described of the general circulation of the ocean, while appropriate to the time-averaged flow, is inadequate for describing the instantaneous flow. There are large variations of currents and of surface height that, instantaneously, can mask the time-averaged picture.

The altimetric and drifter data can be analyzed to yield statistics of the time variability. For example, if the sea surface height is $\eta(x,y,t)$, then we can write

$$\eta(x,y,t) = \overline{\eta}(x,y) + \eta'(x,y,t)$$

where the overbar denotes a long time average and η' is the instantaneous departure of η from the average. An impression of the magnitude of these variations and their geographical distribution can be obtained by mapping the variance of surface height about the time mean defined as

$$\sigma_\eta = \sqrt{\overline{\eta'^2}}. \tag{9.17}$$

The global map is shown in Fig.9.19(bottom). There are distinct maxima of σ_η in regions of strong flow — in the western boundary currents of the Gulf

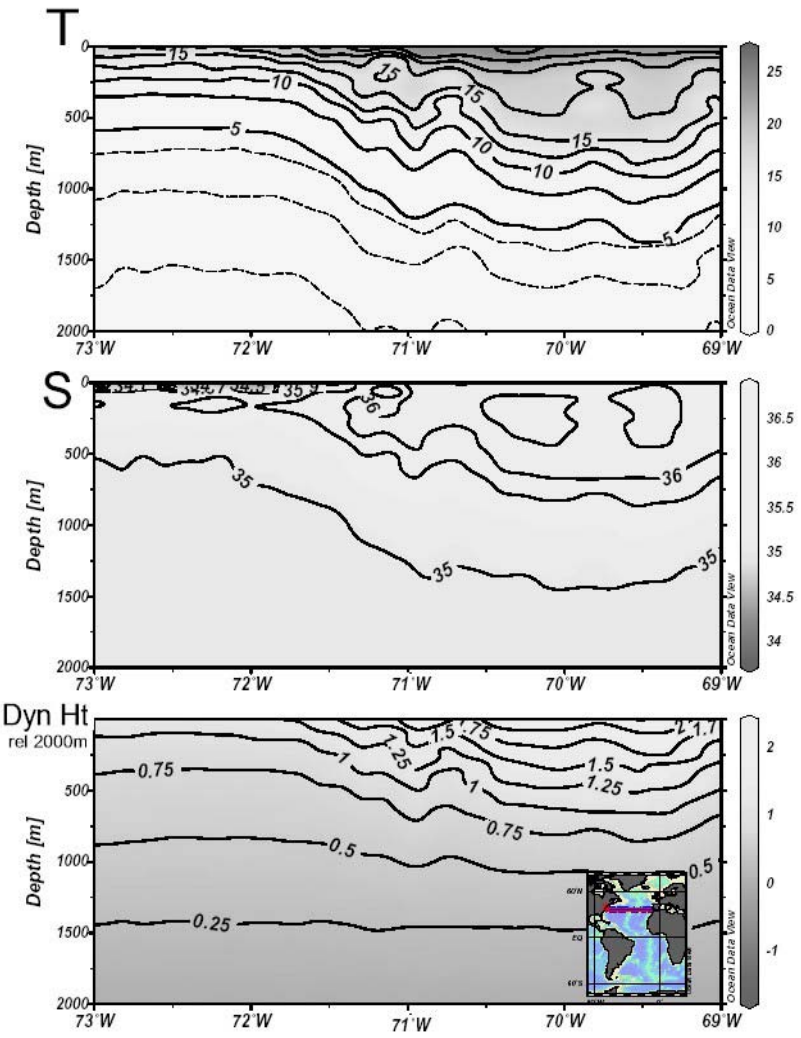

Figure 9.21: Top: Temperature section (in °C) over the top 2 km of the water column crossing the Gulf Stream along 38°N, between 69°W and 73°W (as marked on the inset). Middle: Salinity (in psu) across the same section. Bottom: Dynamic height, $\mathcal{D}$ (in m) computed from Eq.(9.16) relative to 2 km. Produced using Ocean Data View.

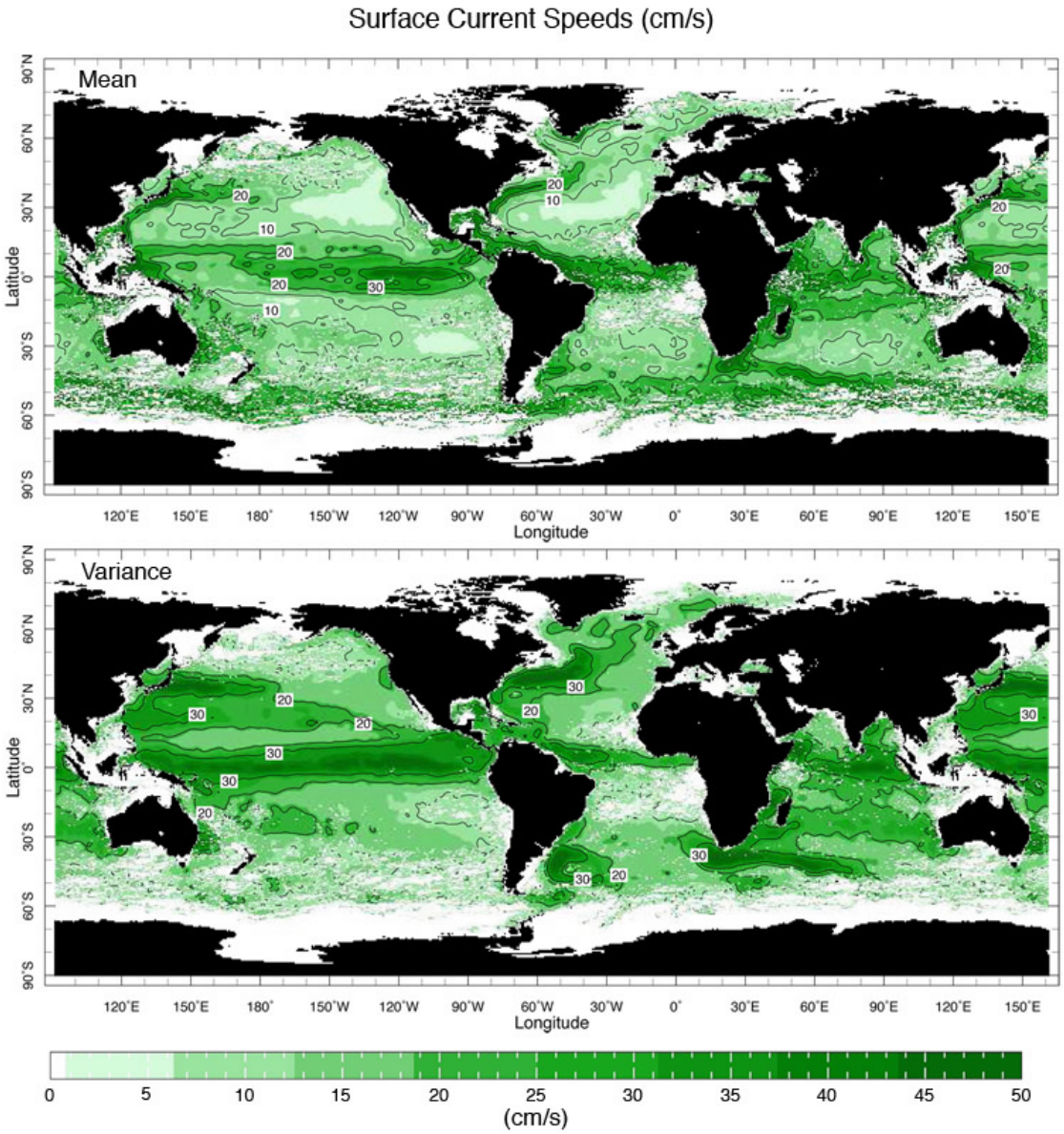

Figure 9.22: (Top) Mean surface drifter speeds, $\sigma_{\overline{u}} = \sqrt{(\overline{u}^2 + \overline{v}^2)^{\frac{1}{2}}}$, and (bottom) eddy drifter speeds, $\sigma_{u'} = \sqrt{\left(\overline{u'^2} + \overline{v'^2}\right)^{\frac{1}{2}}}$ computed from 20 y of drifter observations. Regions of the ocean in which observations are sparse — particularly in the southern oceans around Antarctica — appear as white gaps. Data courtesy of Maximenko and Niiler (personal communication, 2003).

Stream and Kuroshio and in the Antarctic Circumpolar Current (especially at the southern tip of Africa and south of Australia and New Zealand). In these regions, $\sigma_h > 20\,\mathrm{cm}$, so the temporal variance is not very much less than mean spatial variations seen in the top frame of Fig.9.19. Fig.9.22 shows the mean speed of the surface currents together with eddy speeds based on surface drifter data. Mean surface currents in the middle of the gyres are less than $10\,\mathrm{cm\,s^{-1}}$, but note how eddy speeds considerably exceed the mean almost everywhere. This implies that the instantaneous flow can be directed opposite to the time-mean flow. Note also how the tropical variability very evident in drifter observations, Fig.9.22, is less evident in the surface elevation field measured by altimetry, Fig.9.19. This is not surprising: geostrophic balance, as expressed by Eq.(9.11), tells us that, for a given current amplitude, the height gradient vanishes as $f \to 0$ near the equator. Of course this is true for both mean and eddy components of the flow.

These observations show us that the ocean is not steady and laminar: rather, just like the atmosphere, it is highly turbulent. Indeed, ocean eddies are dynamically analogous to the baroclinic eddies studied in GFD Lab XI, Section 8.2.2, and can be called 'ocean weather systems'. However, as will be discussed in Section 10.5, because of the weaker vertical stratification in the ocean compared to the atmosphere, these eddies are typically only 100 km in lateral scale, much smaller than their meteorological counterparts. Ocean eddies typically have a lifetime of many months and intense eddies shed by boundary currents such as the Gulf Stream can survive for a year or so.

The SST distribution over the N Atlantic obtained from satellite observations, shown in Fig.9.23, presents an instantaneous picture of ocean variability in the region of the Gulf Stream. There is a strong gradient of SST across the Gulf Stream which exhibits large meanders and undulations, some of which break off to form closed eddies ("warm core rings" to the north of the stream and "cold core rings" to the south). The eddies and rings have a scale of 100 km or so. In Section 10.5 their formation by the baroclinic instability of the thermal wind shear associated with the substantial temperature gradient across the Gulf Stream will be discussed. Fig.9.21, a hydrographic section across the Gulf Stream, shows that there is a strong and systematic gradient of temperature, more-or-less coincident with the main current, extending all the way down to about 1 km depth. Recall the map of the mean currents at 700 m in the north Atlantic in Fig.9.17. The mean spatial gradient of surface height seen in Fig.9.19 and the surface currents observed by drifters, Fig.9.15, is coincident with this temperature gradient.

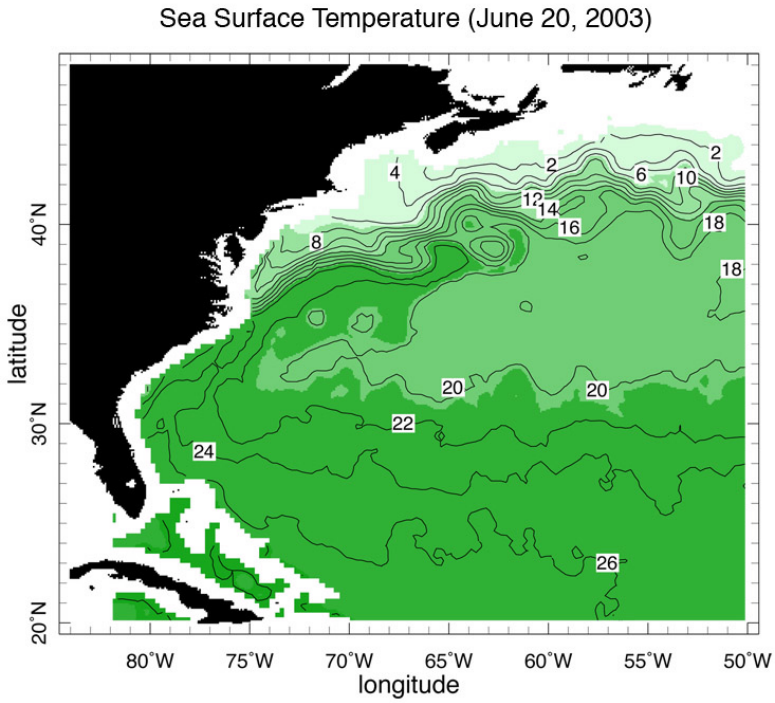

Figure 9.23: A satellite-derived Sea Surface Temperature map (in °C) over the Gulf Stream, from March 26th, 2003. Note the advection of warm tropical waters northwards by the strong western boundary current and the presence of strong meanders and eddies in the seaward extension of the Gulf Stream.

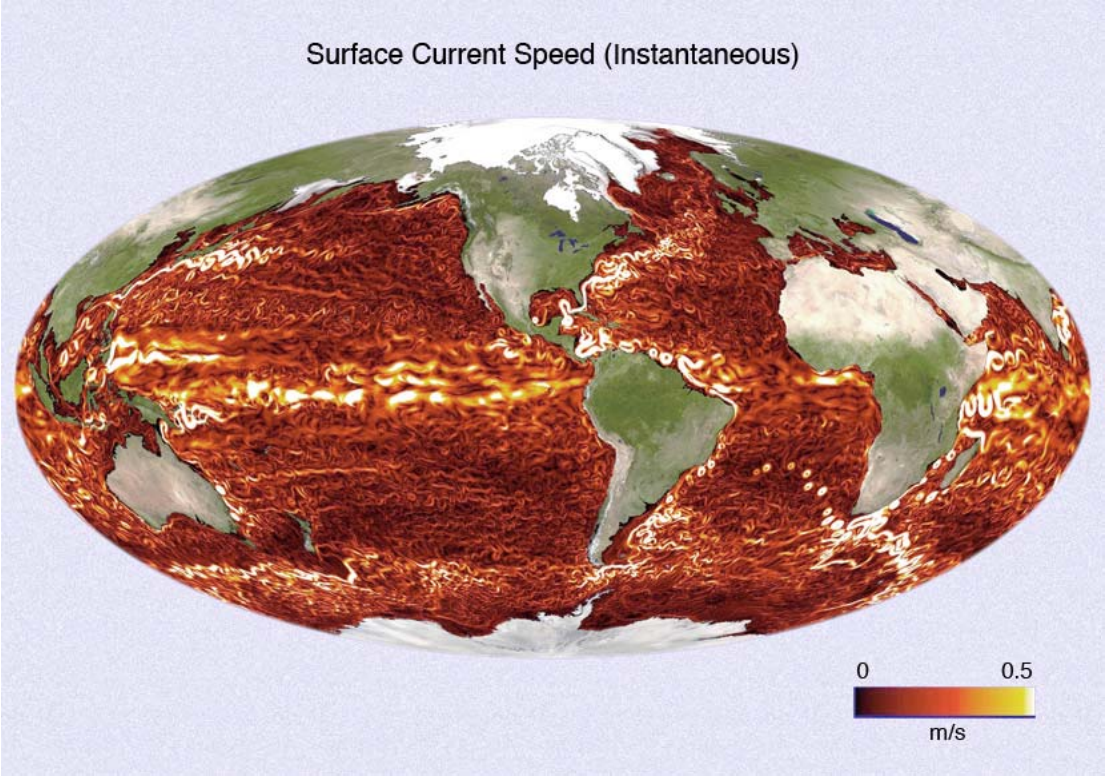

Figure 9.24: Instantaneous map of surface current speed from a global 'eddy-resolving' numerical model of ocean circulation. The scale is in units of $\mathrm{m\,s^{-1}}$. Modified from Menemenlis et al (2005).

High-resolution numerical simulations also give a vivid impression of what the real ocean is probably like; near-surface current speeds in a numerical model are shown in Fig.9.24. Again, we see large-amplitude spatial variations characteristic of eddy motions in the western boundary and circumpolar currents. Just as in the observations, Fig.9.22, there is also much eddy activity straddling the equator.

9.5 Further reading

Reviews of the physical properties of seawater and a description of the large-scale circulation of the ocean can be found in Pickard and Emery (1990).

A more advanced text which reviews the underlying dynamical principles is Pond and Pickard (1983). Another useful introductory resource is the Open University text on Ocean Circulation. Stommel's (1965) book on the Gulf Stream is an excellent and very accessible account of ocean dynamics in the context of the observations.

9.6 Problems

1. Consider an ocean of uniform density $\rho_{ref} = 1000$ kg m^{-3}.

   (a) From the hydrostatic relationship, determine the pressure at a depth of 1 km and at 5 km. Express your answer in units of atmospheric surface pressure, $p_s = 1000\,\mathrm{mbar} = 10^5\,\mathrm{Pa}$.

   (b) Given that the heat content of an elementary mass dm of dry air at temperature T is $c_pT\ dm$ (where c_p is the specific heat of air at constant pressure), find a relationship for, and evaluate, the (vertically integrated) heat capacity (heat content per degree Kelvin) of the atmosphere per unit horizontal area. Find how deep an ocean would have to be in order to have the same heat capacity per unit horizontal area. (You will need information in Tables 1.4 and 9.3.)

2. Simple models of mixed layers.

   (a) Assume that in the surface mixed layer of the ocean, mixing maintains a vertically uniform temperature. A heat flux of $25\mathrm{W\,m^{-2}}$ is lost at the ocean surface. If the mixed layer depth does not change and there is no entrainment from its base, determine how long it takes for the mixed layer to cool down by 1 °C. [Assume the mixed layer has a depth of 100 m and use data in Table 9.3].

   (b) Consider the development of a simplified, convective, oceanic mixed layer in winter. Initially, at the start of winter, the temperature profile is given by

   $$T(z) = T_s + \Lambda z$$

   where z is depth (which is zero at the sea surface and increases upwards) is depth, and the gradient $\Lambda > 0$.

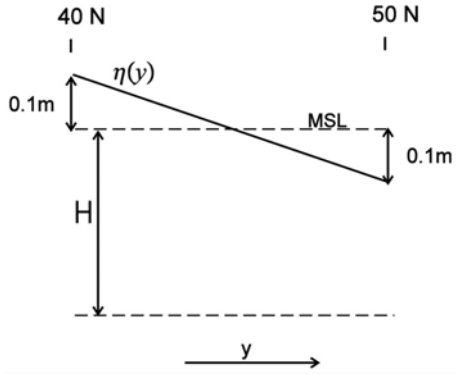

Figure 9.25:

During the winter heat is lost from the surface at a rate Q W m^{-2}. As the surface cools, convection sets in and mixes the developing, cold, mixed layer of depth $h(t)$, which has uniform temperature $T_m(t)$. (Recall GFDlab II, Section 4.2.4). Assume that temperature is continuous across the base. By matching the heat lost through the surface to the changing heat content of the water column, determine how $h(t)$ and $T_m(t)$ evolve in time over the winter period. Salinity effects should be assumed negligible, so density is related to temperature through Eq.(4.4).

(c) If $Q = 25$W m^{-2} and $\Lambda = 10\,^\circ$C per kilometer, how long will it take the mixed layer to reach a depth of 100 m?

3. Consider an ocean of uniform density $\rho_{ref} = 1000$ kg m^{-3}, as sketched in Fig.9.25. The ocean surface, which is flat in the longitudinal direction (x), slopes linearly with latitude (y) from $\eta = 0.1$ m above mean sea level (MSL) at 40°N to $\eta = 0.1$ m below MSL at 50°N. Using hydrostatic balance, find the pressure at depth H below MSL. Hence show that the latitudinal pressure gradient $\partial p/\partial y$ and the geostrophic flow are independent of depth. Determine the magnitude and direction of the geostrophic flow at 45°N.

4. Consider a straight, parallel, oceanic current at 45°N. For convenience, we define the x-and y- directions to be along and across the current,

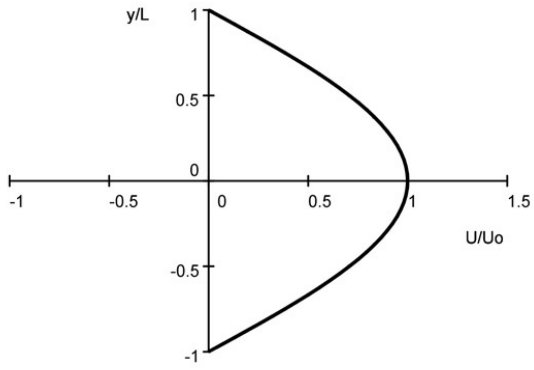

Figure 9.26: A plot of $\frac{u}{U_0}$ at the surface, $z = 0$, against $\frac{y}{L}$.

respectively. In the region $-L < y < L$, the flow velocity is

$$u = U_0 \cos\left(\frac{\pi y}{2L}\right) \exp(\frac{z}{d})$$

where z is height (note that $z = 0$ at mean sea level and decreases downwards), $L = 100\,\mathrm{km}$, $d = 400\,\mathrm{m}$, and $U_0 = 1.5\,\mathrm{m\,s^{-1}}$. In the region $|y| > L$, $u = 0$.

The surface current is plotted in the following figure:

Making use of the geostrophic, hydrostatic and thermal wind relations:

(a) Determine and sketch the profile of surface elevation as a function of y across the current.

(b) Determine and sketch the density difference, $\rho(y, z) - \rho(0, z)$.

(c) Assuming the density is related to temperature by Eq.(4.4) determine the temperature difference, $T(L, z) - T(-L, z)$, as a function of z. Evaluate this difference at a depth of 500 m. Compare with Fig.9.21.

5. Fig.9.21 is a section across the Gulf Stream at 38°N (in a plane normal to the flow), showing the distribution of temperature as a function of depth and of horizontal distance across the flow. Assume for the purposes of this question (all parts) that the flow is geostrophic.

(a) Using hydrostatic balance, and assuming that atmospheric pressure is uniform and that horizontal pressure gradients vanish in the deep ocean, *estimate* the differences in surface elevation across the Gulf Stream (*i.e.*, between 70°W and 72°W). Neglect the effect of salinity on density, and assume that the dependence of density ρ on temperature T is adequately described by Eq.(4.4).

(b) The near-surface geostrophic flow $\mathbf{u}$ is related to surface elevation η by

$$\mathbf{u} = \frac{g}{f}\widehat{\mathbf{z}} \times \nabla\eta \ ,$$

where g is gravity and f the Coriolis parameter. Explain how this equation is consistent with the geostrophic relationship between Coriolis force and pressure gradient.

(c) Assuming (for simplicity) that the flow is uniform down to a depth $D = 500$m, and that the flow is zero below this depth, show that the net water transport (volume flux) along the Gulf Stream at this latitude is

$$\frac{gD}{f}\,\delta\eta \ ,$$

where $\delta\eta$ is the elevation difference you estimated in part (a). Evaluate this transport.

6. Fig.9.27 shows the trajectory of a 'champion' surface drifter which made one and a half loops around Antarctica between March, 1995 and March, 2000 (courtesy of Nikolai Maximenko). Red dots mark the position of the float at 30 day interval.

(a) Compute the mean speed of the drifter over the 5-year period.

(b) Assuming that the mean zonal current at the bottom of the ocean is zero, use the thermal wind relation (neglecting salinity effects) to compute the depth-averaged temperature gradient across the Antarctic Circumpolar Current. Hence estimate the mean temperature drop across the 600 km-wide Drake Passage.

(c) If the zonal current of the ACC increases linearly from zero at the bottom of the ocean to a maximum at the surface (as measured by the drifter), estimate the zonal transport of the ACC through Drake Passage assuming a meridional velocity profile as in Fig.9.26

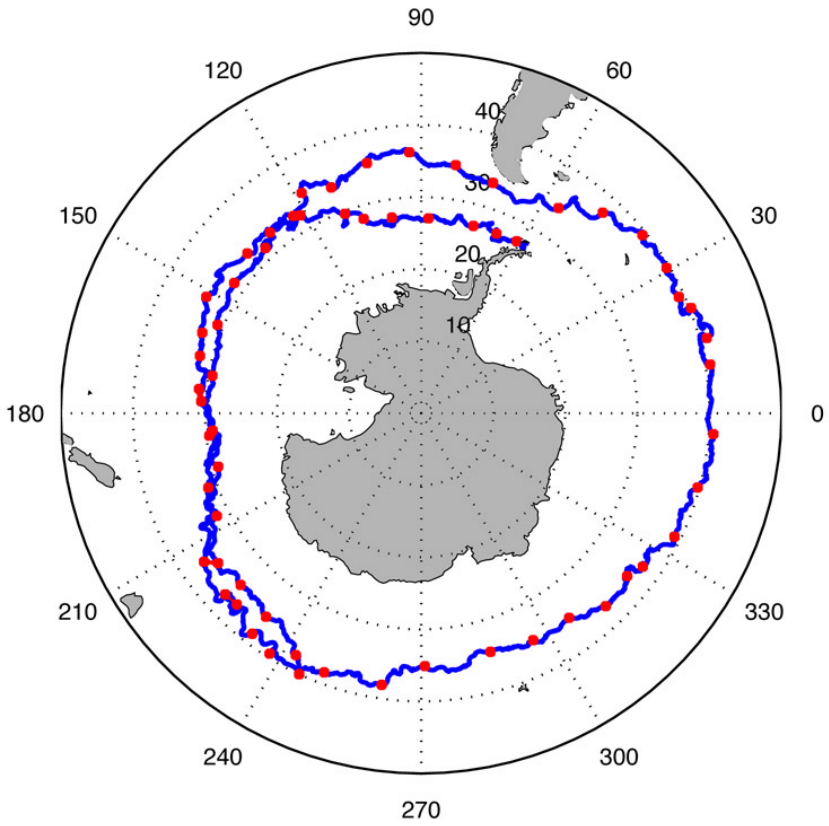

Figure 9.27: The trajectory of a surface drifter which made one and a half loops around Antarctica between March, 1995 and March, 2000 (courtesy of Nikolai Maximenko). Red dots mark the position of the float at 30 day intervals.

and that the depth of the ocean is 4 km. The observed transport through Drake Passage is 130Sv. Is your estimate roughly in accord? If not, why not?